Published in final edited form as:
J Comp Neurol. 2012 February 15; 520(3): 495–527. doi:10.1002/cne.22715.

A Survey of Oral Cavity Afferents to the Rat Nucleus Tractus Solitarii

James Corson[1], **Alexandra Aldridge**[1], **Kristin Wilmoth**[1], and **Alev Erisir**[1]
[1]Department of Psychology, University of Virginia, Charlottesville, VA 22902

Abstract

Visualization of myelinated fiber arrangements, cytoarchitecture, and projection fields of afferent fibers in tandem revealed input target selectivity in identified subdivisions of the nucleus tractus solitarii (NTS). The central fibers of the chorda tympani (CT), greater superficial petrosal (GSP), and glossopharyngeal (IX) nerves, three nerves that innervate taste buds in the oral cavity, prominently occupy the gustatorysensitive rostrocentral subdivision. In addition, CT and IX innervate and overlap in rostrolateral subdivision, which is primarily targeted by the lingual branch of the trigeminal nerve (LV). In rostrocentral subdivision, compared to the CT terminal field in rostrocentral subdivision, GSP appeared more rostral and medial, and IX was more dorsal and caudal. While IX and LV filled the rostrolateral subdivision diffusely, CT projected only to the dorsal and medial portions. The intermediate lateral subdivision received input from IX and LV but not CT or GSP. In the caudal NTS, the ventrolateral subdivision received notable innervation from CT, GSP, and LV, but not IX. No caudal subnuclei medial to solitary tract contained labeled afferent fibers. The data indicate selectivity of fiber populations within each nerve for functionally distinct subdivisions of the NTS, highlighting the possibility of equally distinct functions for CT in the rostrolateral NTS, and CT and GSP in the caudal NTS. Further, this provides a useful anatomical template to study the role of oral cavity afferents in the taste-responsive subdivision of the NTS as well as in subdivisions that regulate ingestion and other oromotor behaviors.

Keywords

Subdivision; Chorda Tympani; Greater Superficial Petrosal; Glossopharyngeal; Gustatory; Taste

Introduction

The nucleus tractus solitarii (NTS) is a major site of peripheral afferent integration to the central nervous system, receiving primary inputs from gustatory, gastrointestinal, cardiovascular, and respiratory receptors, traveling within four cranial nerves: facial, glossopharyngeal, vagus, and trigeminal (Contreras et al., 1982; Norgren, 1983; 1984). A rough topographic organization exists in the nucleus such that, the rostral portion of the NTS receives gustatory information, the intermediate portion receives gastrointestinal information, and the caudal portion receives cardiovascular information (van Giersbergen et al., 1992). The focus of the current study is the orosensory (that is, gustatory, oral mechanosensory, and oral thermosensory) afferents innervating the NTS; the projection patterns of the vagus nerve, which regulates gastrointestinal and cardiovascular functions in the NTS, remain out of the scope of the current study.

Corresponding Author: Alev Erisir; PO Box 400400; Charlottesville, VA 22904.

The primary afferents conveying gustation reach NTS via two branches of the facial nerve, the chorda tympani (CT) and greater superficial petrosal nerves (GSP), and the glossopharyngeal nerve (IX), forming partially overlapping terminal fields (Blomquist and Antem, 1965; Whitehead and Frank, 1983; Hamilton and Norgren, 1984; May and Hill, 2006). Furthermore, each of these nerves is multi-modal, conveying a combination of gustatory, mechanical, and thermal sensitivities, as well as differing stimulus sensitivities for each modality (Nejad, 1986; Harada et al., 1997). While a substantial amount of information has accumulated on the anatomical and electrophysiological properties of orosensory afferents (Hill and Almli, 1980; Ferrell et al., 1981; Whitehead, 1986; Wang and Bradley, 1995; Grabauskas and Bradley, 1996; Harada et al., 1997; Sollars and Hill, 2005; May et al., 2007), endeavors in understanding the functional circuitry of the NTS have been complicated by the fact that these nerves, each carrying multiple sensory modalities, overlap to converge onto functionally heterogeneous cell populations (Davis and Jang, 1988; Bradley and Sweazey, 1992; King and Bradley, 1994; Renehan et al., 1994; 1996). Surveying the level of selectivity of oral cavity afferents for modality-distinct subdivisions will be a useful step in understanding the orosensory circuitry of the NTS.

The CT, GSP, and IX nerves innervate topographically distinct regions of the oral cavity. The majority of CT innervation is from the fungiform taste buds at the front of the tongue and a smaller branch emanates from the anterior foliate papillae at the back of the tongue (Whiteside, 1927; Yamamoto and Kawamura, 1975). GSP innervates the nasoincisor duct and soft palate, and IX innervates the foliate and circumvallate papillae on the posterior tongue. In contrast to CT and GSP nerves, which only innervate taste buds via small diameter myelinated and unmyelinated fibers, IX is a mixed nerve that contains nociceptors (peptidergic, small diameter fibers), large diameter mechanorecetors, and temperature sensitive fibers, which innervate both taste buds and non-gustatory epithelia. All three nerves are responsive to tactile- and temperature-specific stimuli in addition to taste, but whether a specific receptor class conveys each modality for each nerve is unknown (Yamashita and Sato, 1965; Norgren, 1984; Frank, 1991). With regards to chorda tympani thermoreception, it is likely that temperature decreases change the dynamics of a subset of taste receptors, rather than activating a specialized thermo-receptor (Ogawa et al., 1968; Ninomiya, 1996; Lundy and Contreras, 1999). However, a subset of chorda tympani fibers responds exclusively to mechanical stimulation, probably due to channels on the intragemmal endings rather than innervation of the epithelium, while others respond exclusively to taste or to a combination of taste and mechanical stimulation (Biedenbach and Chan, 1971; Matsuo et al., 1995; Smith et al., 2004). Similarly, recording taste responses from individual fibers, Frank (1991) noted that nearly three quarters of glossopharyngeal fibers were sensitive to touch and cooling but not to taste, indicating modality selective heterogeneity.

The NTS is not a homogenous structure, but rather is composed of a number of subdivisions or subnuclei, each with a different cellular composition (Whitehead, 1988; 1990; Kalia and Sullivan, 1982; Herbert et al., 1990), afferent and efferent connectivity, and primary function (King, 2007). Using previously established terminology and border delineation, the subdivisions are as follows: In the rostral one-third of the NTS, the rostrocentral subdivision contains neurons that respond primarily to taste and project to the waist region of parabrachial nucleus (Norgren and Leonard, 1973; Norgren, 1978; Halsell et al., 1996; Williams et al., 1996). Neurons in rostrolateral subdivision mainly respond to tactile information, and project to the external region of the parabrachial nucleus (Norgren, 1978; Whitehead, 1990; Halsell et al., 1996; Halsell and Travers, 1997). The medial subdivision may integrate gustatory and viscerosensory information (Beckman and Whitehead, 1991; King, 2007), and the ventral subdivision may serve as an oromotor center linked to the incoming gustatory information and contains neurons that project to the subjacent reticular

formation (Travers, 1988; Halsell et al., 1996; King, 2007; Nasse et al., 2008). Note that these projection and functional distinctions are generalizations; there is overlap in most of the output pathways and modalities associated with each subdivision. For instance, NTS to PBN projection neurons are most concentrated in the rostrocentral subdivision (Norgren and Leonard, 1973; Travers, 1988; Whitehead, 1990), although labeled neurons were noted in the rostrolateral and ventral subdivisions following retrograde tracer injections in the PBN (Halsell et al., 1996). The caudal two thirds of the NTS receives innervation mainly from the vagus nerve and processes viscerosensory information (e.g. respiratory, gut, etc.) within multiple subnuclei (Herbert et al., 1990; van Giersbergen et al., 1992). Briefly, the medial and commissural subnuclei are involved in cardiovascular regulation, the lateral portion that contains ventrolateral subdivision and intermediate subnuclei is involved in respiratory regulation, and the medial and central portions are involved in gastrointestinal regulation (van Giersbergen et al., 1992).

The primary purpose of this study was to create a normative template of the subdivisional organization of the rat CT, GSP, IX, and the lingual trigeminal (LV) nerves for use in future studies of the modality-selective organization of NTS afferents, as well as developmental and lifespan plasticity observed in this nucleus. In order to investigate the compartmentalized organization of CT, GSP, IX, and LV in the NTS, we labeled each nerve with biotinylated dextran amines and compared the terminal field label with histologically identified subdivisions in adjacent sections throughout the anterior-posterior extent of the NTS. While CT, GSP, and IX project to the rostrocentral subdivision, particular selectivity of each nerve for different subnuclei was evident.

Methods

Animals

Twelve adult female (postnatal 50–60 days) Sprague Dawley rats (Harlan) were used for afferent projection atlases in this study. Six additional rats were used for optimization of histological stains and for horizontal plane sections or they were excluded from further processing due to failed tracer injections. All animals were kept on a 12:12 light:dark cycle and fed standard rat chow. All experiments were carried out in accordance with the regulations of the Animal Care and Use Committee of the University of Virginia.

Nerve Labeling and Tissue Preparation

Groups of 3 animals underwent nerve labeling surgery for CT, GSP, IX, or LV. Afferent nerves were labeled via application of lyophilized dextran crystals to the transected nerve similar to previously published studies (Sollars and Hill, 2000; May and Hill, 2006; Mangold and Hill, 2007). Briefly, animals were anesthetized with medetomidine/ketamine (0.2mg/kg, 20mg/kg; IM), secured in a non-traumatic head holder (Erickson, 1966), and a ventral approach taken to access the chorda tympani or greater superficial petrosal nerve within the tympanic bulla. The glossopharyngeal nerve was accessed using the same ventral approach as for CT and GSP, but the nerve was located ventral and medial to the tympanic bulla. The lingual-trigeminal nerve was located rostral to the tympanic bulla, central to the separation of the chorda tympani from the lingual nerve. For GSP and CT, a small hole was made in the tympanic bulla and the nerve transected peripheral to the geniculate ganglion. CT was located running lateral to the cochlea and posterior to the tensor tympani muscle. GSP was located under (dorsal) the junction of the tensor tympani muscle with the skull, anterior to the cochlea. As only a single nerve was labeled in each animal and the nerves join centrally after the geniculate ganglion, unintentional labeling of both branches of the facial nerve in the same animal was not probable. Crystals of 3kd biotinylated dextran amine (BDA; Invitrogen) were then placed onto the central stump of the cut nerve and the hole in

the bulla covered in parafilm. For IX labeling, the same approach was taken and the bulla exposed but not opened. IX was located medial to the bulla running through connective tissue dorsal to the hypoglossal nerve. IX was transected, and the central stump was placed onto a small piece of parafilm covering the bulla. Following application of 3kd BDA, another piece of parafilm was placed over top of the sectioned nerve and dextran crystals. For trigeminal labeling, the lingual branch of trigeminal was transected centrally to where CT separates from the chorda-lingual nerve. CT was transected in the bulla (but not labeled) prior to the labeling of LV in order to prevent accidental transport of BDA into NTS via CT. LV was placed onto a square of parafilm and BDA applied to the central stump. Following each tracer application procedure, the incision was sutured, the animal was revived with atipamezole (1mg/kg; IM), and a post-operative analgesic (buprenorphine; 0.05mg/kg; SC) was administered.

After 48 hours of survival for tracer transport, animals were given an overdose of sodium pentobarbital, and were euthanized by transcardial fixative perfusion. Perfusates were 100 ml Tyrode's solution (137mM NaCl, 5.5mM Dextrose/Glucose, 1.2mM $MgCl_2$, 2mM KCl, 0.4mM NaH_2PO_4, 0.9mM $CaCl_2$, 11.9mM $NaHCO_3$, in 1L dH20) delivered in 2–3 minutes followed by 300mls of 4% paraformaldehyde in 0.1M PB (pH 7.4) at room temperature. Brains were post-fixed overnight at 4°C in the same fixative.

Tracer Visualization and Histological Staining

Brains were blocked 2 mm anterior to the cerebellar peduncle, and sectioned coronally using a vibratome (Leica VT1000S) at 50μm in three series: one for nerve label visualization, one for Nissl staining, and the third for myelin staining. Sequential order of sections was maintained for all subsequent processing. For visualization of BDA, sections were incubated in avidin-biotin complex with 0.1% Triton in 0.01M phosphate buffer saline (PBS, pH 7.4) overnight at 4°C. The sections were then rinsed 5×5 minutes in PBS and reacted in 0.1% diaminobenzidine in PBS with 0.001% H_2O_2 for 5 minutes. The sections were then mounted onto subbed slides, allowed to dry overnight, and finally dehydrated and coverslipped. Sections that would undergo histological staining were mounted onto subbed slides immediately after sectioning. Nissl staining was achieved by progressively rehydrating the slides in decreasing concentrations of ethanol followed by 0.5% cresyl violet in dH_2O with 0.3% acetic acid. The sections were then dehydrated, the stain cleared in 95% ethanol, and the slides coverslipped with DPX. For myelin staining, either commercially available Black Gold II (Millipore, Billerica, MA) or a previously published protocol using gold hydrochloride (Schmued, 1990; Schmued and Slikker, 1999) was used. For the latter, sections mounted onto subbed slides were rehydrated in 0.01M PBS for 2 minutes and then incubated in 0.1% $HAuCl_4$ in 0.02M PBS (pH 7.0) for 10–12 minutes at 60°C. The sections were monitored using a light microscope for the desired degree of impregnation every 2–3 minutes. After fine myelination within NTS subdivisions (see Results) was differentiated, the slides were incubated in 0.1% $KAuCl_4$ in saline (pH 7.0) for 3 minutes at 60°C. Following 2×2 minutes rinses in 0.01M PBS, the slides were incubated in 1% sodium thiosulfate in dH_2O at 60°C for 3 minutes, rinsed 5×3 minutes in 0.01M PBS, dehydrated, and coverslipped.

Imaging and Alignment of Sections

Nissl, myelin, and tracer-stained sections were photographed at two magnifications using a Leica light microscope (model 888011) equipped with a Leica DC200 1.0 megapixel digital camera at 192×1536 resolution. Each myelin- and Nissl-stained section was imaged once through a 2.5× objective to include the entire section, and again through a 5× objective to capture landmark details of NTS and surrounding fields. Adjacent fields of each tracer-labeled section were then photographed at 10× (typically 8–10 frames). Using the Adobe

Photoshop layers function, these 10× images were tiled, aligned under visual guidance, and stitched to construct a composite of the entire projection field. Then, using Adobe Illustrator, lower magnification images were enlarged by digital re-sampling so that unmanipulated higher magnification images could be aligned and merged. This allowed for examination of the NTS at a higher resolution while still being able to use multiple landmarks to align the sections to adjacent myelin- and Nissl-stained material. Then, the images of three adjacent sections, one with each stain, were layered and aligned onto each other using opacity and transform tools of Illustrator. Additional transparent layers on top were used for drawing the NTS outline, solitary tract, and subdivision borders. By tuning the visibility of each Illustrator layer, it was possible to superimpose the same outlines onto the aligned myelin, Nissl, and tracer labeled sections. Within each image triplet, the myelin-stained section was used to draw the majority of the subdivision borders as well as the solitary tract. The Nissl-stained section was then used to confirm that the subdivisions represented not only delineation based on myelination, but also cellular packing density. The NTS outline and subdivision borders were then superimposed onto the terminal field label in question and the fiber distribution was examined in relation to the NTS architecture. Because each triplet represented a 150μm tissue block (i.e. three 50μm sections), the landmark outlines transposed onto tracer labeled sections represent an anterior-posterior precision of ±100μm. For higher-magnification tracer labeled images, adjacent fields containing the labeled fibers (typically 30–40 fields for each final image) were photographed using a 40× objective and stitched together in Photoshop constructing a high-resolution composite of the entire projection field.

Subdivision Nomenclature

The nomenclature and subdivision border criteria used in previously published work (Whitehead, 1988; Barry et al., 1993; Halsell et al., 1996) were adhered to as much as possible. In determining subdivision borders in myelin- and Nissl-stained sections, we relied on qualitative observations rather than quantitative measurements, such as fiber density, soma size distributions, or cell packing density.

Preparation of Figures

Images captured using Image Pro Plus (v5.1; MediaCybernatics, MD, USA), applying white-field background subtraction to remove concentric aberrations in the image field. Adjacent images are manually tiled in Adobe Photoshop, and the figures were prepared using Adobe Illustrator. Image manipulations were limited to minor midrange adjustments to match the grayscale levels across panels, if needed.

Results

The entire series from each brain was analyzed to identify anatomical landmarks corresponding to NTS subdivisions, as well as the extent of axonal projections from the four afferents within these subdivisions.

Identification of NTS and its subdivisions

Adjacent Nissl- and Myelin-stained sections were examined to detect reliably identifiable tissue landmarks relative to a standardized coordinate template, which would allow us to correlate afferent innervation patterns and NTS subdivisions. The cytoarchitectural criteria for NTS and subdivision borders described by previous investigators (Whitehead, 1988; Barry et al., 1993; Halsell et al., 1996) were consulted to confirm the nomenclature and the utility of landmarks identified in material prepared as described in this study. For ease of comparison with previous studies, it should be noted that conventionally, NTS is arbitrarily divided into two or three rostrocaudal levels, depending on focus of interest. Both schemas

define the rostral level as extending from the rostral pole to where NTS touches the 4th ventricle (Whitehead, 1988). While three-level schema divides remainder of NTS into intermediate (4th ventricle junction to obex) and caudal (obex to spinal cord junctions) levels (Kalia and Sullivan, 1982; Herbert et al., 1990), orosensory/gustatory focused two-level scheme labels NTS caudal to 4th ventricle junction as caudal. In the current study, we have used the nomenclature of two-level NTS schema, although the coordinate template we used is suitable for matching landmarks in both.

NTS borders—Adjacent series of myelin- and Nissl-stained sections were useful in identifying complementary features of cellular architecture of the brainstem (Figure 1–2). Myelin staining invariably delineated the dorsal and medial borders of the NTS and the bundles of axons that traverse the nucleus at several orientations, including those making up the solitary tract. Similar to what is noted in previous studies (Whitehead, 1988; Travers and Norgren, 1995; Halsell et al., 1996), the rostral, lateral, and ventral borders of the NTS were more ambiguous, even with the histological stains (Figure 1E–F, 2E–F, 3–4). Anterior-posterior traversing myelinated axon bundles, similar to those of the subjacent reticular formation, were also present within the ventral subdivision, making the delineation of the two difficult at times. While the density of the fine myelinated fibers surrounding these anterior-posterior traversing bundles most often was greater in the subjacent reticular formation than the ventral subdivision, the ventral border of NTS should be regarded conjectural throughout this study. Similarly, the lateral border of the NTS was identified as an increase in the density of fine myelination between the lateral subdivision and the matrix region of the medulla and trigeminal-solitary transition zone (Figures 1–5). As the lateral subdivision is already densely packed with fine myelinated fibers, this transition was often subtle, but was identifiable in all animals examined. Regardless, in all cases analyzed, abovementioned criteria were applied for drawing NTS outlines, rather than imposing a prototypical template. Further, due to ambiguity of the ventral and lateral borders of NTS, medial and rostral borders were relied on as landmarks throughout the study, including for standardizing NTS location within the brainstem across different animals. Although difficult to discern in isolation, the rostral pole of the NTS was readily identified by disappearance of typical NTS myelination pattern (dorsoventrally traversing medium thickness myelin bundles through a region that contains no myelinated fibers) when serial sections though NTS were examined in a posterior to anterior order.

Subdivision borders—In identifying the subdivision borders, Nissl and myelin stains were again used in conjunction with each other. The medial subdivision was identified in Nissl-stained sections as a less cell-dense area directly medial to the central subdivisions (Figures 1D and 2D, 3–4). Nissl staining was used in identifying the border between the central and lateral subdivisions of rostral NTS (Figures 1D, 3); the former contains smaller, densely packed, round or elongate cells, and the latter contains sparse cells with pale cytoplasm. The border between rostrocentral and rostrolateral subdivisions was also readily visible from the myelin-stained material with the central subdivision containing a relative paucity of fine myelinated fibers when compared to the dense network of fine myelination in the lateral subdivision (Figures 1B, 3–4). Unlike in rostral NTS, the subdivisions of caudal NTS, as described in detail previously (Kalia and Sullivan, 1982; Herbert et al., 1990), were best identified in Nissl-stained sections. These subdivisions were noted as encountered (Figures 2D&F, 4H), yet not outlined for simplicity as no selective afferent fibers were encountered there (see below). Myelin staining was very useful in providing reliable and easily detectable landmarks for comparisons of afferent patterns. For example, myelinated fiber pattern that characterizes rostrolateral subdivision was also detectable in more caudal levels as a distinct region lining the medial border of the solitary tract. As the dorsoventrally traversing myelinated bundles disappear (around AP +500), fine myelination becomes a

prominent landmark, dividing the NTS axially into two sheets (medial unmyelinated and lateral myelinated) throughout the caudal two thirds of the nucleus (Figures 4C–G). The lateral border of this fine myelinated strip coincides with the medial envelope of the solitary tract in the middle third of the NTS and the medial border of ventrolateral subdivision in the caudal third (Figures 2B and E, 4E–G). At sections close to AP +0, the strip of tissue between this landmark border and the medial envelope of solitary tract contains intermediate subnucleus that is identifiable in Nissl sections (Figure 4 F–H; Herbert et al., 1990). In further caudal sections, this fine myelinated strip remains detectable even in the lack of solitary tract envelope, although we weren't able to make further subdivision identifications based on Nissl staining at those levels. This myelination pattern provides a reliable landmark for mapping different brains within a uniform template, and it consistently delineates a zone that is not innervated by the four afferent nerves examined in this study (see below). If charted, the medial border of this strip appears as a continuation of the rostrolateral/rostrocentral subdivision border, and thus it may be analogous to the caudolateral division identified in the hamster and mouse (Whitehead, 1988; Zaidi et al., 2008). As the NTS progressed caudally, the ventral subdivision was architectonically congruous with the ventrolateral subdivision; therefore, no V-VL border was identified in our material. The point at which the NTS meets the 4th ventricle was operatively defined as the transition point between the ventral and ventrolateral subdivisions, and between the rostrocentral subdivision and the caudal subnuclei (Figure 4A–B), following previously used conventions (Whitehead, 1988; Travers and Norgren, 1995; Herbert et al., 1990). It is understood that any border identified in a histochemically stained section would not transfer exactly on the adjacent sections because NTS and subdivision borders do not progress perpendicular to coronal plane of the brain.

Throughout this manuscript, the anatomical landmarks of the NTS are conveyed using a coordinate system in which the most anterior brain section that contained area postrema (AP; Figure 5E1) was designated as the "zero point". Thus, every section has a unique anterior-posterior number relative to AP with the most anterior 50μm vibratome section containing AP being designated "AP = 0". Using this system, the coordinates of major landmarks throughout the NTS extent were consistently stereotyped. It should be noted that, the thickness of vibratome sections, thus the margin of error for the AP coordinate measurements form each brain, was 50μm. The rostral pole of the NTS (Figure 5A), as identified as the disappearance of the less densely myelinated NTS relative to the vestibular and reticular formation and the ventral-lateral extension of the spinal vestibular nucleus, was located 2367 ± 100μm (mean ± SD; n=9) from AP = 0. The NTS-4th ventricle junction (Figure 2D), as identified as the anterior-most section where the NTS borders the lateral wall of the fourth ventricle and caudal to the prepositus nucleus, was located 833 ± 97μm (mean ± SD; n=9) from AP = 0. At this operationally defined landmark, there were no identifiable architectonic criteria to distinguish the rostrocentral and rostrolateral subdivisions from their caudal counterparts. However, afferent projection patterns offered an insight (see below), revealing presence of further NTS subdivisions located at the intermediate regions of the nucleus (also noted in Whitehead and Frank, 1983 and Herbert et al., 1990). No attempt was made to identify the caudal pole of the NTS. Our particular interest was in the subdivisions in the rostral NTS, where orosensory processing takes place, but the caudal NTS was also thoroughly examined to chart the locations of labeled afferent fibers.

The biotinylated dextran amine placed at cut nerves peripheral to the ganglia resulted in anterograde filling of axons and terminal boutons in the NTS (Figures 6–9). Also stained were retrogradely filled cells representing the motor component of the cranial nerve. While the dendrites of these neurons often projected dorsally into the terminal field of the labeled nerve (most prominently for IX), this only occurred in the rostral-most sections. At high magnifications, it was clear that even in these regions dense terminal field was still present,

therefore we found this potential confound negligible. The labeling pattern resulting from each nerve was similar across repeated experiments. No other unspecific label was present. Images of sections containing tracer label were overlaid on adjacent myelin and Nissl labeled sections to identify afferent axon terminations in identified subdivisions of the NTS (Figures 1E–F and 2E–F).

Comparison of coronal and horizontal planes: Afferent innervation to NTS in adult and postnatal animals has been studied extensively, using mostly horizontal sections (May and Hill, 2006; Sollars et al., 2006; Mangold and Hill, 2007; 2008; Thomas and Hill, 2008). Using a horizontal plane to study NTS is advantageous because the entire NTS can be sampled in fewer sections than with coronal planes (500–600μm in horizontal vs. 3000μm in coronal planes). Furthermore, dendrites of most gustatory neurons are oriented parallel to the horizontal plane (Davis and Jang, 1988; King and Bradley, 1994; Suwabe and Bradley, 2009), rendering studies involving afferent target relations feasible. Disadvantages of horizontal sections stem from the fact that while most NTS subdivisions are oriented parallel to dorsal surface of the nucleus, the dorsal surface itself progresses rostrally in a lateral and ventral incline. As a result, horizontal sections are not amenable to construct a coordinate-based representation of the NTS. An example of this is illustrated in Figure 6, where the representation of the rostral NTS expands anteriorly as the horizontal sections become more ventral. That is, the most anterior portions of dorsal horizontal sections do not represent most rostral NTS.

In order to be able to relate our coronal section based coordinate system to studies that utilize horizontal sectioning, we stained a horizontal NTS series containing typical planes to study gustatory NTS for myelin, and compared myelin identified subdivision landmarks in these sections to those in coronal sections (Figure 6). The NTS-4th ventricle junction, clearly identifiable in both horizontal and coronal planes, was used to transfer coordinate measurements in coronal sections onto horizontal sections. Furthermore, fine myelination that is used as the landmark to draw the border between rostrocentral and rostrolateral subdivisions was detectible medial to solitary tract in dorsal sections (Figure 6A3–B3) and lateral to the solitary tract in ventral sections (Figure 6C3–D3). Due to the unique orientation of horizontal sections, the rostrolateral subdivision, best viewed in coronal sections between about AP+1800μm and AP+1000μm, is prominently present in even the most ventral horizontal planes (see E2 markings in Figure 6A2–D2). This might have led to the attribution of inputs in the horizontally sliced rostrolateral subdivision to the ventral NTS. We also noted that ventrolateral subdivision, which contains substantial CT and GSP fibers may not have been sampled in typical horizontal sections that are used to study gustatory NTS, because this subdivision is located so much further caudal to the prominently dense terminal field of the rostrocentral and rostrolateral subdivisions.

Afferent axon labeling in NTS subdivisions

CT projections—Labeled CT axons are found approaching NTS following the course of cranial nerve VII, as delineated in Paxinos atlas, and entering NTS proper dorsally at the medial-lateral midpoint within 500μm posterior to the rostral pole (Figure 7A–D). At the entry point, a bundle of myelinated axons turns medially to form the densest termination zone in the rostrocentral subdivision (Figures 11A, 12A–B, 13A–B). In addition to the rostrocentral group of terminations, bouton-bearing CT axons spread within the rostrolateral, ventral, and ventrolateral subdivisions. At the level of the densest rostrocentral projections, relatively sparser, yet prominent and distinctly bouton-bearing axons are present in the rostrolateral subdivision (Figures 7C, 12A–B). These projections arise from a bundle of axons separate from those that enter the rostrocentral subdivision, turning laterally to reach the solitary tract (Figure 11B). There, they project ventrally where they contort to form an L-

shape, filling the dorsal and medial halves of the rostrolateral subdivision (Figures 7C, 12A). A major portion of this second group of CT fibers then travels as a dorsal bundle within the solitary tract for about 1 mm caudal to AP=0 (Figure 7C–H). None of the labeled fibers within the solitary tract displayed boutons. These axons that travel within the solitary tract most likely lead to the terminal field that is observed in ventrolateral subdivision (Figure 7G–L). At the anterior-posterior level that rostrocentral fields greatly dissipate, sparse CT fibers now become evident ventral and medial to the solitary tract, surrounding a CT-free region (Figures 7E–F, 14A–B, 15A–B). Because the region that is surrounded by these sparse CT fibers is distinct from rostrocentral and rostrolateral subdivisions, and the subnuclei of the caudal NTS, it will be referred to as the intermediate lateral subdivision (Figures 14A–B, 15A–B, arrows). No histo-architectural differentiation was noted for intermediate lateral subdivision in sections without CT (and GSP, see below) label. The CT fibers that outline the ventral portion of the intermediate lateral subdivision are continuous with another group of terminations that are prominent throughout the caudal NTS, in the ventrolateral subdivision (Figures 7G–L, 15A–B). In fact, out of the 4 nerves examined for this study, CT axons provided the densest terminal field in the ventrolateral subdivision (Figures 16–18). Thus, there are three main subdivisions that contain CT fiber terminations: rostrocentral, rostrolateral, and ventrolateral. Efferent axons and their respective salivatory nucleus projecting neurons are located medial and ventral to the rostral pole of the NTS.

GSP projections—Like CT axons, GSP axons arrive at the NTS within tract of n. facialis, and enter the NTS at an aspect slightly lateral to the CT axons (Figures 8B–C, 12C). The terminal field pattern closely resembles that of CT, with a few exceptions. As with CT, bouton-bearing GSP fibers are densest in the rostrocentral subdivision, dissipating about 300μm from the NTS-4th ventricle junction (Figure 8E–F). In contrast to CT axons, which fill the lateral 2/3 of the rostrocentral subdivision, GSP fibers are densest in the middle 1/3 and sparse in the lateral 1/3 of the rostrocentral subdivision (Figures 8B–D, 12C–D, 13C–D). Similar to CT, a group of GSP axons travels caudally within the solitary tract (Figure 8D–K) traversing the caudal extent of the NTS and innervating the ventrolateral subdivision. Also similar to CT, at coronal levels where rostrocentral fibers become sparse, a group of GSP fibers (Figure 8E–F) define the medial and ventral borders of the intermediate lateral subdivision (Figures 14C–D, 15C–D), which is devoid of GSP innervation. These lateral GSP fibers appear continuous with the ventrolateral projections that span the entire caudal NTS (Figures 8E–K, 14C–D). Unlike CT, except for a few fibers bordering the rostrocentral subdivision, GSP fibers are relatively absent within the rostrolateral subdivision, (Figures 8C–E, 12C–D, 13C–D). Thus, there are two main groups of GSP fibers: the dense rostrocentral terminations and relatively sparse ventrolateral terminations. As with CT, efferent fibers and neurons are located medial and ventral to the rostral pole of the NTS.

IX projections—IX myelinated bundles enter the brain by passing laterally through the inferior cerebellar peduncle and spinal trigeminal tract, and emerge to travel medially toward NTS at the level of NTS-4th ventricle junction. Here, they join in the solitary tract and give off bouton bearing branches in both the rostral and the caudal NTS, as well as in the interstitial nucleus (Kalia and Sullivan, 1982) within the solitary tract. The largest IX labeled fascicule travels rostrally at the dorsal aspect of the solitary tract to give off terminal fields within the rostrocentral and rostrolateral subdivisions (Figures 9C–E, 12E–F, 13E–F). Once in the NTS, a large bundle of bouton-free fine axons courses medially and envelops the dorsal portion of the rostrocentral subdivision (Figures 9F–G and 19). In contrast to CT and GSP, the subjective density of IX terminations in the rostrocentral subdivision does not surpass that in the rostrolateral, resulting in a more medio-laterally uniform terminal field, with very little spread into the subjacent ventral subdivision (Figures 9C–F, 12E–F, 13E–F). Within the rostrocentral subdivision, the rostral-most IX fibers are sparsely located at around

300μm from the rostral pole, occupying mainly the dorsal 2/3 of the subdivision. The terminal field fills the majority of the caudal half of the rostrocentral subdivision and the medial 2/3 of the rostrolateral subdivision. At the caudal-most portions of the rostrocentral subdivision, IX fibers appear denser than CT and GSP terminal fields (Figures 7E, 8E, 9E). At approximately the anterior-posterior level of the NTS-4th ventricle junction, IX axons fill the intermediate lateral subdivision (Figures 9F, 14E–F, 15E–F); a region clearly avoided by CT and GSP terminations. Interestingly, a large IX fascicle travels through the solitary tract from approximately AP -450μm throughout the rostral extent of the solitary tract (Figure 9D–I), yet only significant terminal field is found rostral to AP +450μm (Figure 9G). No IX fibers are found in the ventral or ventrolateral subdivisions, except for a small terminal field immediately lateral to the solitary tract at the caudal-most extent of IX terminal field (Figures 9G, 16E–F); this zone may be part of the interstitial nucleus. Thus, IX axons mainly give terminal boutons in rostrolateral, rostrocentral and intermediate lateral subdivisions. Similar to CT and GSP, IX efferent projecting neurons are located medial to the rostral pole of the NTS, however since tracer label is visualized every 150μm in our material, we cannot directly compare fine distribution of these neurons at anterior-posterior coordinates, as others have (Contreras et al., 1980).

LV projections—Numerous labeled LV fiber bundles project medially from the spinal trigeminal tract into the NTS at all rostral-caudal levels, though densest portion of the terminal field was located rostral to AP +650μm (Figure 10A–G). As LV axons enter NTS from its lateral aspect, they travel lateral to medial before terminating at their target sites; thus, LV axons run lateral to medial across the solitary tract, but do not travel within anterior-posterior bundles (Figure 10G–H). At the rostral pole, scant terminal field is observed in the NTS, while dense terminal field is present throughout the dorsomedial spinal trigeminal nucleus directly lateral to the NTS (Figure 10A–B). Between the rostral pole and the NTS-4th ventricle junction, dense LV terminal field fills the rostrolateral subdivision with only scant labeling in the ventral subdivision (Figures 10C–F, 12G–H, 13G–H, 14G–H). The LV axon labeling in rostrolateral subdivision does not fill the entire subdivision; in fact, trigeminal fibers clearly avoid a clearly demarcated region at the ventral-lateral one-third of the rostrolateral subdivision (Figure 10C–D, 12G). Interestingly, the same region is also avoided by IX and CT fibers (Figure 12E and 12A), suggesting either further segmentation in rostrolateral subdivision, or extension of the ventral subdivision more dorsal than drawn here. Histological sections do not offer any landmarks to verify either of these possibilities. The rostrocentral subdivision does not contain any labeled fibers, however, very sparse labeling is located at the transition between the rostrocentral subdivision and the subnuclei of the caudal NTS (Figures 10F–G, 15G, 16G), suggesting the presence of another distinct zone that surrounds caudal aspect of the rostrocentral subdivision. It should be noted that CT, GSP, and IX also send fibers to this region. Denser labeling can be found in the intermediate lateral subdivision (Figure 15F–G). In the ventrolateral subdivision LV fibers are very sparse and irregular (Figures 10H–L, 16G–H, 17G–H, 18G–H), mostly enveloping the lateral border of NTS, even though a large fiber bundle enters NTS directly at this caudal level (Figure 10I–J).

Discussion

The innervation patterns of three nerves that carry orosensory information inclusive of taste (CT, GSP, and IX) and one nerve exclusive of taste (LV) are examined, and territory selectivity within NTS subdivisions is revealed (See Figure 20 for summary). The main conclusions are: 1) CT projects to rostrocentral and rostrolateral subdivisions in the rostral NTS, and to ventrolateral subdivision in the caudal NTS. 2) GSP projects to rostrocentral and ventrolateral subdivisions. 3) IX projects to rostrocentral, rostrolateral, and intermediate lateral subdivisions, and the interstitial nucleus along the solitary tract. 4) LV projects

almost exclusively to rostrolateral and intermediate lateral, with sparse fibers in the ventrolateral subdivision. 5) The dorsal half of the rostrocentral subdivision is targeted by CT, GSP, and IX. The dorsal and medial halves of rostrolateral subdivision are targeted by CT, IX, and LV, while IX and LV also innervate more ventral portions of this subdivision. The intermediate lateral subdivision is targeted by IX and LV, and the ventrolateral subdivision of the caudal NTS is targeted by CT, GSP, and LV. 6) Within the rostrocentral and rostrolateral subdivisions, each nerve occupies a discrete, yet overlapping territory, suggesting oral topography- and/or modality-based selectivity.

This paper provides a systematic examination of the afferent innervation of the rat NTS in relation to architectonic subdivisions identified by myelin and Nissl stains in tandem. Past research revealed detailed information on the cytoarchitectural landmarks of NTS subdivisions using cell size, packing density, and dendritic properties of the neurons (Davis and Jang, 1988; Whitehead, 1988). The projection patterns of afferent nerves within NTS have been investigated in detail in monkey (Beckstead and Norgren, 1979), rat (Contreras et al., 1982; Hamilton and Norgren, 1984; May and Hill, 2006), and hamster (Whitehead and Frank, 1983), however a correlation of projection patterns with architectonically identified subdivisions was lacking. Our work using anterograde tract tracing, which allows differentiation of bouton bearing fibers from axons of passage, confirms and extends these earlier works by revealing the projection patterns of bouton-bearing fibers within these NTS subdivisions. The present study alludes to a functional heterogeneity for each nerve, indicating a selectivity of fiber populations within each nerve for functionally distinct subdivisions of the NTS. This provides a useful anatomical template to study the role of oral cavity afferents in the taste-specialized rostrocentral subdivision as well as subdivisions that regulate ingestion, respiration, and other oromotor behaviors.

Identification of Subdivision Borders

Earlier studies have divided the rat NTS into lateral and medial subdivisions based on cell packing density both in the rostral and caudal halves of the nucleus (Torvik, 1956; Hamilton and Norgren, 1984). Subsequent work using reduced silver and Golgi staining, revealed a central subdivision (Whitehead, 1988) which was later identified as the prominent region for gustatory activation (McPheeters et al., 1990; Harrer and Travers, 1996; Travers and Hu, 2000). Based on cellular packing and morphology, as well as myelinated fiber arrangement, the rostral portion is further divided into medial, central, lateral, and ventral subdivisions (Whitehead, 1988). With this scheme, the anterior-most point at which the NTS borders 4th ventricle arbitrarily divides the nucleus into rostral and caudal halves. While studies with an orosensory focus in hamster and mouse divided the caudal NTS into medial, central and lateral divisions (Whitehead 1988; Zaidi et al., 2008), the subnuclei in the caudal two-thirds of the rat NTS was also described in detail (Herbert et al., 1990). Therefore, the subdivision nomenclature used in the current study incorporated terminology from both orosensory and cardiovascular/respiratory focused studies. Based on Nissl differentiation and distinct efferent projection patterns, the NTS caudal to the 4th ventricle junction contains multiple subnuclei including medial, parvicellular, intermediate and commissural subnuclei that process general viscerosensory information, and ventrolateral, intermediate and caudal commissural subnuclei, which receive respiratory and upper airway afferents. With the exception of ventrolateral division, all caudal subnuclei as identified by Herbert et al (1990) criteria, were devoid of afferent fibers from four nerves studied. The histological staining used in the present study was amenable to reliably differentiate subdivisions located in both the rostral and caudal divisions of the NTS. Specifically, the cell body arrangement found in Nissl-stained sections was used to determine the border between the rostrocentral (smaller cells, tighter packing) and medial (larger cells, looser packing) subdivisions. Myelin staining revealed a dense plexus of fine myelinated fibers that fills the lateral NTS, demarcating the

borders between the rostrocentral and rostrolateral subdivisions. Similarly, the ventral subdivision in the rostral NTS and the ventrolateral subdivision in the caudal NTS were readily distinguished on the basis of streams of transversely sectioned myelinated bundles continuous with the reticular formation. Although previous investigators have identified a further compartmentalization within the ventrolateral subdivision (Kalia and Sullivan, 1982; Kalia et al., 1984a; Kalia et al., 1984b; Altschuler et al., 1989), our material was not sufficient in revealing any discernable borders.

We chose to use the anterior-most section containing area postrema as our "zero point" as it is readily identifiable in all sections regardless of histological stain, and is approximately 720μm anterior to obex (according to Paxinos and Watson, 2009; also see Hamilton and Norgren, 1984). As such, comparison of our results with previous studies utilizing obex, requires a shift in the anterior-posterior coordinate. While obex is an extremely useful landmark for physiological recordings (it is visible with the cerebellum intact) our "zero point" is significantly closer to our area of interest. While we run the risk of losing the most anterior remnants of area postrema through sectioning, mounting, and tissue processing, we found the distances of this "zero point" to NTS landmarks (e.g. anterior pole and 4th ventricle junction) consistent between animals, thus proving to be suitable for NTS coordinate mapping.

While the histological landmarks in our material did not indicate presence of subdivisions other than medial, rostrocentral, rostrolateral and ventral in the rostral NTS, termination patterns of the four nerves revealed the likelihood of additional subdivisions at the rostral to caudal transition region. Specifically, at coronal sections anterior to NTS-4th ventricle junction, a collection of prominent CT and GSP fibers outline the medial and ventral borders of a region within histologically identified rostrolateral subdivision. Furthermore, this region that was selectively avoided by CT and GSP was densely innervated by IX and LV. It is unlikely that the ventral half, which contains CT and GSP fibers, belongs to caudal NTS subdivisions because, in further caudal sections, where caudal intermediate subnucleus and other caudal subnuclei are more unequivocally identified (Herbert et al., 1990), labeled fibers (from any of the four labeled afferents) are not present. Despite the lack of information as to whether a functionally distinct subdivision exists at rostral-caudal NTS transition levels, it is convenient to have a name for this region that receives exclusively IX and LV boutons. Thus, we refer to it as the intermediate lateral subdivision. The intermediate lateral subdivision identified in our work is rostral to the caudal NTS subnuclei identified in Herbert et al (1990) and Kalia and Sullivan (1982), and it is located at the caudal limits of the rostral NTS. In our material, we cannot distinguish whether the CT and GSP axons that outline the intermediate lateral subdivision are extensions of sparse fibers that surround dense rostrocentral projections, or rostral portions of ventrolateral projections that extend through the caudal NTS. Regardless, the intricate selective patterning of CT, GSP, IX, and LV axons outside of rostrocentral subdivision herald the complexity of the involvement of orosensory information in viscerosensory regulation.

Afferentation Patterns and Comparisons to Previous Studies

Visualization of afferent fibers in the NTS is not novel; many past studies have identified projection patterns of nerves originating in the oral cavity using degeneration (Torvik, 1956), HRP (Whitehead and Frank, 1983; Hamilton and Norgren, 1984), or fluorescent tracer approaches (May and Hill, 2006). The general pattern of afferent projections revealed in the current study is in complete agreement with past work describing innervation of rostral NTS with orosensory fibers. However, our work underlines an important discrepancy, indicating that the topographic overlap of CT and IX afferents in rostrocentral subdivision is more extensive than previously indicated. A main advantage of the tracer used in the current studies was its sensitivity to fill the projection field entirely and without any

background, and its capacity to discriminate nerve bundles, axonal branches of various caliber and terminal boutons. These, along with concurrent subdivision identification, allowed us to confirm several selectivity patterns that are indicated in past studies, and are crucially relevant for orosensory circuitry: GSP projections avoid rostrolateral subdivision; CT has an extensive (although not as dense as in rostrocentral) field in rostrolateral subdivision, which also contains IX and LV fields; IX has an extensive field in both rostrocentral and rostrolateral subdivisions; and in caudal NTS, CT and GSP have substantial projection fields in ventrolateral subdivision. Past studies have also indicated a topographic selectivity for CT, GSP and IX fields within rostral NTS (Hamilton and Norgren, 1984; Whitehead, 1988; Whitehead and Finger, 2008), and this is most demonstrative in studies that utilized multiple fluorescent tracers in the same animals (May and Hill, 2006). In particular, Hamilton and Norgren (1984) indicated a parcellation of NTS with afferent innervations such that CT almost completely dominate more rostral aspects, while IX dominates two thirds of the rostral NTS and extend into caudal divisions. The discrepancy between that conclusion (Hamilton and Norgren, 1984, Figure 6; Whitehead and Finger, 2008) and the current study (Figure 20) may stem from several factors. First, while HRP, degeneration, and PHAL approaches may be selective for thicker fibers, and larger terminals, BDA effectively visualizes finer fibers, and minimizes the de-emphasis of sparser projections. With this, in addition to the higher imaging resolution, we were able to demonstrate the wider extent of CT/IX overlap in rostrocentral subdivision, which was also evident in dual labeling studies (May and Hill, 2006). Second, in comparison to the exceptionally dense CT projection within the anterior rostrocentral subdivision, CT fibers become much sparser (to the extend that individual fibers can be visualized in 50μm sections) in more posterior rostrocentral subdivision. By placing emphasis on NTS subdivisions as distinct entities, we did not attempt to analyze the density or importance of inputs within individual subdivisions, and as such reported whether or not a subdivision receives input from a particular afferent nerve. With that, we believe our summary figure more fairly illustrates the extent of overlap between CT and IX projections throughout the rostral NTS. Furthermore, closely spaced photographs of raw data in the current study provided a visual display of selective topography of afferents within each subdivision, particularly the topographic selectivity between GSP (medial) and CT (lateral) fields in rostrocentral, and between CT (dorsal) and IX (ventral) fields in rostrolateral subdivisions. In sum, our results corroborate past findings, and extend them in providing a detailed template for predicting the NTS sites, in which orosensory afferents, individually and through possible convergence, may contribute to the activity of neural circuitries within NTS subdivisions.

Functional Implications

The afferent branches of the facial nerve, CT and GSP, are broadly considered to carry primarily taste information (Whitehead and Finger, 2008), although mechanosensory (Biedenbach and Chan, 1971; Matsuo et al., 1995; Smith et al., 2004) and thermosensory (Ogawa et al., 1968; Ninomiya, 1996; Lundy and Contreras, 1999) activation have been documented. Along these lines, their most intense terminal fields are found in rostrocentral subdivision, which contains neurons responding to tastant stimulation of the oral cavity (McPheeters et al., 1990; Harrer and Travers, 1996; Travers and Hu, 2000). Although additional projections from these nerves in lateral and caudal subdivisions of the NTS have been noted (Contreras et al., 1982; Whitehead and Frank, 1983; Whitehead, 1988), these projections are largely ignored, probably due to their sparseness in comparison to their exceptionally dense presence in the rostrocentral subdivision. Our material revealed that a substantial portion of CT terminal field in the rostral NTS is located within the rostrolateral subdivision, suggesting a strong contribution to the firing properties of neurons within.

Similarly, the intensity of the labeled fibers in the ventrolateral subdivision indicates that CT and GSP activation should have a notable contribution to neuronal responses there.

Does CT bring a functionally uniform input across NTS subdivisions? If CT carries taste information to all of the subdivisions it innervates, stimuli optimized for gustatory function should elicit responses in rostrolateral and ventrolateral NTS just as in rostrocentral. In one study, no tastant induced c-fos activation was found outside of the rostrocentral subdivision in the rat (Harrer and Travers, 1996). However, a subsequent study revealed c-fos activation in other subdivisions, though the majority of c-fos activity remained in the rostrocentral subdivision (Travers and Hu, 2000). This discrepancy is largely attributed to differences in sample sizes and adaptation periods to the behavior paradigm, but may also be due to inconsistencies in the control of somatosensory and thermosensory aspects of the stimulation. Neither study investigated activation in the caudal NTS, thus leaving the functional identification of these extra-rostrocentral terminal fields undetermined from c-fos studies. Furthermore, retrograde tracer injections in the gustatory region of parabrachial nucleus prominently fill the cells in the rostrocentral subdivision, and to a lesser extent the rostrolateral and ventral subdivisions (Halsell et al., 1996). However, this region of the parabrachial nucleus also responds to somatosensory stimulation, making the interpretation of the relayed orosensory modality ambiguous. The caveats to these results strongly indicate that CT projections outside of the rostrocentral subdivision may mediate activity other than taste, and that the exclusivity of CT activity for gustatory function needs to be scrutinized in general.

It should be noted that the evidence for the lack of gustatory responses in subdivisions other than rostrocentral is equally inconclusive. First, a comprehensive physiological analysis of gustatory-evoked activity in NTS subdivisions has yet to be undertaken. The detailed physiology studies in the past only stimulated anterior tongue and was focused on developing a tastant topographic map (McPheeters et al., 1990). Other studies investigating oral cavity topography in the NTS (Travers and Norgren, 1995) demonstrated a medial-lateral division of taste and tactile responses in the NTS, but did not include a subdivisional analysis. Additionally, c-fos studies unavoidably necessitated the use of sub-optimal stimuli, because stimulation with salts did not consistently produce fos-activity in the NTS, and only high concentrations of sucrose and quinine reliably elicited c-fos labeling. As such, these studies unavoidably focused on the topographic differentiation of sapid vs. aversive stimuli rather than global gustatory function. Therefore, the presence of gustatory-evoked activity in regions other than the rostrocentral subdivision cannot be definitively negated.

The functional analysis of nerve response characteristics has revealed substantial heterogeneity, much of which is not well understood. Even though, CT, GSP, and IX are sensitive to taste, mechanical, and temperature stimulation, little is known with regards to the multi-modal receptor innervation of single nerve fibers or the distribution of these fibers within the NTS. With regards to the chorda tympani nerve, heterogeneity of rat ganglion cell sensitivities for different tastants (Lundy and Contreras, 1999; Breza et al., 2006; Breza et al., 2010) and orosensory modalities (Biedenbach and Chan, 1971; Matsuo et al., 1995; Smith et al., 2004), as well as the heterogeneity of axon morphologies (Holland and Robinson, 1992) are well documented. Although there is no evidence to suggest heterogeneity of CT fibers at the level of taste bud innervation, CT nerve recordings indicate distinct populations of taste and mechanosensitive fibers (Matsuo et al., 1995). While it is not known whether any particular axonal morphology correlates with such functional diversity, the faster conduction velocity of mechanosensitive fibers (Matsuo et al., 1995) suggests that these impulses are brought to NTS via axons with larger diameter and/or thicker myelination. The central distribution of these mechanosensitive fibers is unknown. Indeed, anterior tongue tactile stimulation activates the lateral portion of the NTS (Travers

and Norgren, 1995), although this cannot be directly attributed to CT because this region also receives substantial LV input (Hamilton and Norgren, 1984). Thus, further investigation into the morphological ultrastructure of these rostrolateral CT afferents will likely provide insights into the nerve's functional diversity.

Dysgeusia is a well-documented distortion of the sense of taste that can be caused by iatrogenic chorda tympani damage during middle ear surgery (House, 1963; Gopalan et al., 2005; Michael and Raut, 2007). It is also recognized that iatrogenic CT damage also lead to symptoms other than those related to taste, including tingling, pain, and numbness, suggesting that CT may also confer general sensation (Costen et al., 1951). Recent studies provided further evidence that this nerve was also responsible for carrying the activity for pain, temperature, and two-point discrimination (Perez et al., 2006), showing that general sensory loss can occur after CT damage. These authors proposed that general sensation deficits are due to chorda tympani-trigeminal cross talk, which can occur through converging afferentation of these two nerves. Our findings, illustrating substantial CT innervation in the trigeminal (along with glossopharyngeal) dominated rostrolateral subdivision, are in agreement with the hypothesis that CT conveys general sensory information, and may contribute to processing of touch and pain sensation in this mechanosensory dominant NTS subdivision.

In an extensive primary afferent study of the hamster NTS, Whitehead and Frank (1983) speculated on the function of CT projections to the caudal NTS, suggesting that different taste qualities may be represented at different rostral-caudal levels in the hamster NTS. Caudal CT projections may also bring integrative taste information regarding these specific qualities to predominantly viscerosensory subnuclei. Similar to this earlier work that documented the occurrence of CT projections in the caudal NTS, the current analysis highlights the selectivity and the extent of these projections, however, the response properties of caudal NTS neurons to CT stimulation and whether caudal GSP projections convey a similar function are not known.

What is the function of orosensory fibers in gastrointestinal specialized central NTS and cardiovascular specialized caudal NTS? Because the oral cavity is the beginning of both the alimentary and the respiratory tracts, it is conceivable that orosensation contributes in some way to regulation of both functions. Swallowing is a complicated action that requires orchestration of over 50 pairs of muscles (Cunningham and Sawchenko, 1990), and sensory stimulation at the oral cavity is considered vital for the procurement, formation, and transportation of all ingested food (Martin, 2009; Steele and Miller, 2010). Initiation of swallowing is primarily mediated by the superior laryngeal nerve, with possibly a multi-synaptic involvement from IX fibers (Jean, 2001). Furthermore, the chemical stimulus, particularly a sour taste, facilitates reflex swallowing from the pharynx (Kajii et al., 2002) via interneurons activated by orosensory inputs terminating in rostral subdivisions. The central NTS subdivision at the anterior-posterior level of the NTS-4th ventricle junction provides medullary inputs to nucleus ambiguus, which contains esophageal motor neurons (Cunningham and Sawchenko, 1990; 2000). In our material, while sparse fibers from CT and GSP were present at the rostrocentral/centrocentral transition region, we found no evidence for monosynaptic orosensory input to central subdivisions that project to nucleus ambiguus. In contrast, CT and GSP form substantial terminal fields, indicative of monosynaptic connections, throughout the ventrolateral NTS, a subdivision that receives vagal input and mediates pulmonary function (Kubin et al., 2006). While our material does not allow identification of all caudal subdivisions, the region that receives these connections corresponds to the ventrolateral subdivision in which lung vagal fibers from slowly adapting stretch receptors terminate (Kubin et al., 2006). Cells in this subdivision project to the parabrachial region, contributing to the integration of pulmonary function with other neural

systems, including the voluntary control of breathing. Possible functions of orosensory inputs from the anterior mouth may include the sensation of airflow through the oral cavity while mouth-breathing, suppression of breathing while preparing to swallow, and signaling the presence of fluids in the mouth to constrict the larynx and to protect lungs from aspiration (Miller, 2002; Matsuo and Palmer, 2009).

Implications of Afferent Field Overlap

Previous work has revealed a substantial overlap among CT, GSP, and IX projection fields in the rat rostral NTS (May and Hill, 2006), suggesting a functional convergence among these afferents. The present study extends these finding by revealing that CT and IX fibers overlap in rostrolateral subdivision and all three overlap in the rostrocentral subdivision. It is possible that the subdivision selectivity for afferent overlap in rostral NTS reflects the spatial overlap of the oral cavity regions each of these afferents innervates. CT and GSP overlap in their innervation of the anterior oral cavity (tongue and nasoincisor duct, respectively) and all three nerves overlap in the posterior oral cavity (CT on the foliate papillae, IX on the foliate and circumvallate papillae, and GSP on the soft palate). Therefore, oral cavity topography may explain the partial field-overlap patterns of the three nerves in the rostrocentral subdivision, but not when rostral NTS is regarded as a whole. Lack of GSP innervation in the rostrolateral subdivision rather suggests that topographic selectivity may be present in each subdivision independently: In the rostrolateral subdivision IX overlaps and exceeds CT projection field at the ventral half of this region. Another, although certainly not mutually exclusive, possibility is that the subdivision selectivity of overlapping afferents reflects a specificity for the type of sensory information (i.e. gustatory vs. mechanosensory) conferred by each nerve; the rostrocentral subdivision receiving taste-specific fibers from all three nerves and the rostrolateral receiving the tactile- and/or pain-specific fibers carried in the chorda tympani and glossopharyngeal nerves. The demonstration of selectivity and exclusivity of each subdivision, and of the inputs they receive, for such discrete sensory processing domains awaits a comprehensive mapping of NTS subdivisions for taste and touch stimuli in systematically deafferented animals.

The chorda tympani, greater superficial petrosal, glossopharyngeal, and trigeminal nerves innervate the subdivisions of the nucleus of the solitary tract in discrete, yet overlapping patterns. This specificity underlies the possibility for multi-modal (e.g. taste and tactile) as well as uni-modal integration from multiple oral cavity regions in the rostrocentral, rostrolateral, and ventrolateral subdivisions. It is through this comprehensive examination of the subdivisional terminal field distribution that we will be able to better qualify and quantify changes in orosensory nerve innervation during development and after sensory perturbation.

Acknowledgments

We thank Drs. David Hill, Ruth Stornetta, and Patrice Guyenet from University of Virginia for sharing their expertise and providing insightful comments.

Funding Source: NIH-NIDCD 1R56DC010183-01 (AE) & NIH-NIDCD 1R01DC010183-01 (AE)

List of Abbreviations

NTS	nucleus tractus solitarii
st	solitary tract
AP	area postrema

4V	fourth ventricle
CT	chorda tympani nerve
GSP	greater superficial petrosal nerve
IX	glossopharyngeal nerve
LV	lingual branch of trigeminal nerve
PBN	parabrachial nucleus

NTS Subdivisions

RC	rostrocentral subdivision
RL	rostrolateral subdivision
V	ventral subdivision
M	medial subdivision
IL	intermediate lateral subdivision
VL	ventrolateral subdivision

Abbreviations in Figure 5

MVe	medial vestibular nucleus
SpVe	spinal vestibular nucleus
mlf	medial longitudinal fasciculus
Gi	gigantocellular reticular nucleus
py	pyramidal tract
PCRt	parvicellular reticular nucleus
sp5	spinal trigeminal tract
Sp5	spinal trigeminal nucleus
ml	medial lemniscus
ts	tectospinal tract
IO	inferior olivary nuclei
ROb	raphe obscurus nucleus
10N	dorsal motor nucleus of the vagus
12N	hypoglossal nucleus
CC	central canal
Amb	nucleus ambiguus
LRt	lateral reticular nucleus
IRt	intermediate reticular nucleus
Cu	cuneate nucleus
Gr	gracile nucleus

MD	medullary reticular nucleus
Mx	matrix region of the medulla
5Sol	trigeminal-solitary transition zone
Pr	prepositus nucleus
X	nucleus X
IS	inferior salivatory nucleus
RN	raphe nuclei
DC	dorsal cochlear nuclei
8cn	cochlear root of the 8th nerve
icp	inferior cerebellar peduncle
7N	facial nucleus

References

Altschuler SM, Bao XM, Bieger D, Hopkins DA, Miselis RR. Viscerotopic representation of the upper alimentary tract in the rat: sensory ganglia and nuclei of the solitary and spinal trigeminal tracts. The Journal of comparative neurology. 1989; 283(2):248–268. [PubMed: 2738198]

Barry MA, Halsell CB, Whitehead MC. Organization of the nucleus of the solitary tract in the hamster: acetylcholinesterase, NADH dehydrogenase, and cytochrome oxidase histochemistry. Microsc Res Tech. 1993; 26(3):231–244. [PubMed: 8241561]

Beckman ME, Whitehead MC. Intramedullary connections of the rostral nucleus of the solitary tract in the hamster. Brain research. 1991; 557(1–2):265–279. [PubMed: 1747757]

Beckstead RM, Norgren R. An autoradiographic examination of the central distribution of the trigeminal, facial, glossopharyngeal, and vagal nerves in the monkey. The Journal of comparative neurology. 1979; 184(3):455–472. [PubMed: 106071]

Biedenbach MA, Chan KY. Tongue mechanoreceptors: comparison of afferent fibers in the lingual nerve and chorda tympani. Brain research. 1971; 35(2):584–588. [PubMed: 5135555]

Blomquist AJ, Antem A. Localization of the Terminals of the Tongue Afferents in the Nucleus of the Solitary Tract. The Journal of comparative neurology. 1965; 124:127–130. [PubMed: 14304268]

Bradley RM, Sweazey RD. Separation of neuron types in the gustatory zone of the nucleus tractus solitarii on the basis of intrinsic firing properties. Journal of neurophysiology. 1992; 67(6):1659–1668. [PubMed: 1629769]

Breza JM, Curtis KS, Contreras RJ. Temperature modulates taste responsiveness and stimulates gustatory neurons in the rat geniculate ganglion. Journal of neurophysiology. 2006; 95(2):674–685. [PubMed: 16267112]

Breza JM, Nikonov AA, Contreras RJ. Response Latency to Lingual Taste Stimulation Distinguishes Neuron Types Within the Geniculate Ganglion. Journal of neurophysiology. 2010 Epud ahead of print.

Contreras RJ, Beckstead RM, Norgren R. The central projections of the trigeminal, facial, glossopharyngeal and vagus nerves: an autoradiographic study in the rat. J Auton Nerv Syst. 1982; 6(3):303–322. [PubMed: 7169500]

Contreras RJ, Gomez MM, Norgren R. Central origins of cranial nerve parasympathetic neurons in the rat. The Journal of comparative neurology. 1980; 190(2):373–394. [PubMed: 7381063]

Costen JB, Clare MH, Bishop GH. The transmission of pain impulses via the chorda tympani nerve. Ann Otol Rhinol Laryngol. 1951; 60(3):591–609. [PubMed: 14885902]

Cunningham ET Jr. Sawchenko PE. Central neural control of esophageal motility: a review. Dysphagia. 1990; 5(1):35–51. [PubMed: 2202557]

Cunningham ET Jr, Sawchenko PE. Dorsal medullary pathways subserving oromotor reflexes in the rat: implications for the central neural control of swallowing. The Journal of comparative neurology. 2000; 417(4):448–466. [PubMed: 10701866]

Davis BJ, Jang T. A Golgi analysis of the gustatory zone of the nucleus of the solitary tract in the adult hamster. The Journal of comparative neurology. 1988; 278(3):388–396. [PubMed: 2464006]

Erickson R. Nontraumatic headholders for Mammals. Physiol Behav. 1966; 1(1):97–98.

Ferrell MF, Mistretta CM, Bradley RM. Development of chorda tympani taste responses in rat. The Journal of comparative neurology. 1981; 198(1):37–44. [PubMed: 7229140]

Frank ME. Taste-responsive neurons of the glossopharyngeal nerve of the rat. Journal of neurophysiology. 1991; 65(6):1452–1463. [PubMed: 1875254]

Gopalan P, Kumar M, Gupta D, Phillipps JJ. A study of chorda tympani nerve injury and related symptoms following middle-ear surgery. J Laryngol Otol. 2005; 119(3):189–192. [PubMed: 15845189]

Grabauskas G, Bradley RM. Synaptic interactions due to convergent input from gustatory afferent fibers in the rostral nucleus of the solitary tract. Journal of neurophysiology. 1996; 76(5):2919–2927. [PubMed: 8930244]

Halsell CB, Travers SP. Anterior and posterior oral cavity responsive neurons are differentially distributed among parabrachial subnuclei in rat. Journal of neurophysiology. 1997; 78(2):920–938. [PubMed: 9307125]

Halsell CB, Travers SP, Travers JB. Ascending and descending projections from the rostral nucleus of the solitary tract originate from separate neuronal populations. Neuroscience. 1996; 72(1):185–197. [PubMed: 8730716]

Hamilton RB, Norgren R. Central projections of gustatory nerves in the rat. The Journal of comparative neurology. 1984; 222(4):560–577. [PubMed: 6199385]

Harada S, Yamamoto T, Yamaguchi K, Kasahara Y. Different characteristics of gustatory responses between the greater superficial petrosal and chorda tympani nerves in the rat. Chemical senses. 1997; 22(2):133–140. [PubMed: 9146903]

Harrer MI, Travers SP. Topographic organization of Fos-like immunoreactivity in the rostral nucleus of the solitary tract evoked by gustatory stimulation with sucrose and quinine. Brain research. 1996; 711(1–2):125–137. [PubMed: 8680855]

Herbert H, Moga MM, Saper CB. Connections of the parabrachial nucleus with the nucleus of the solitary tract and the medullary reticular formation in the rat. The Journal of comparative neurology. 1990; 293(4):540–580. [PubMed: 1691748]

Hill DL, Almli CR. Ontogeny of chorda tympani nerve responses to gustatory stimuli in the rat. Brain research. 1980; 197(1):27–38. [PubMed: 7397561]

Holland GR, Robinson PP. Axon populations in cat lingual and chorda tympani nerves. J Dent Res. 1992; 71(8):1468–1472. [PubMed: 1506513]

House HP. Early and Late Complications of Stapes Surgery. Arch Otolaryngol. 1963; 78:606–613. [PubMed: 14059356]

Jean A. Brain stem control of swallowing: neuronal network and cellular mechanisms. Physiol Rev. 2001; 81(2):929–969. [PubMed: 11274347]

Kajii Y, Shingai T, Kitagawa J, Takahashi Y, Taguchi Y, Noda T, Yamada Y. Sour taste stimulation facilitates reflex swallowing from the pharynx and larynx in the rat. Physiol Behav. 2002; 77(2–3):321–325. [PubMed: 12419408]

Kalia M, Fuxe K, Hokfelt T, Harfstrand A, Lang RE, Ganten D. Distribution of neurophysin II immunoreactive nerve fibers within the subnuclei of the nucleus of the tractus solitarius of the rat. Brain research. 1984a; 321(1):71–82. [PubMed: 6388732]

Kalia M, Fuxe K, Hokfelt T, Johansson O, Lang R, Ganten D, Cuello C, Terenius L. Distribution of neuropeptide immunoreactive nerve terminals within the subnuclei of the nucleus of the tractus solitarius of the rat. The Journal of comparative neurology. 1984b; 222(3):409–444. [PubMed: 6199382]

Kalia M, Sullivan JM. Brainstem projections of sensory and motor components of the vagus nerve in the rat. The Journal of comparative neurology. 1982; 211(3):248–265. [PubMed: 7174893]

King, MS. Anatomy of the Rostral Nucleus of the Solitary Tract. In: Bradley, RM., editor. The Role of the Nucleus of the Solitary Tract in Gustatory Processing. 2007.

King MS, Bradley RM. Relationship between structure and function of neurons in the rat rostral nucleus tractus solitarii. The Journal of comparative neurology. 1994; 344(1):50–64. [PubMed: 8063955]

Kubin L, Alheid GF, Zuperku EJ, McCrimmon DR. Central pathways of pulmonary and lower airway vagal afferents. J Appl Physiol. 2006; 101(2):618–627. [PubMed: 16645192]

Lundy RF Jr, Contreras RJ. Gustatory neuron types in rat geniculate ganglion. Journal of neurophysiology. 1999; 82(6):2970–2988. [PubMed: 10601433]

Mangold JE, Hill DL. Extensive reorganization of primary afferent projections into the gustatory brainstem induced by feeding a sodium-restricted diet during development: less is more. J Neurosci. 2007; 27(17):4650–4662. [PubMed: 17460078]

Mangold JE, Hill DL. Postnatal reorganization of primary afferent terminal fields in the rat gustatory brainstem is determined by prenatal dietary history. The Journal of comparative neurology. 2008; 509(6):594–607. [PubMed: 18546275]

Martin RE. Neuroplasticity and swallowing. Dysphagia. 2009; 24(2):218–229. [PubMed: 19130130]

Matsuo K, Palmer JB. Coordination of Mastication, Swallowing and Breathing. Jpn Dent Sci Rev. 2009; 45(1):31–40. [PubMed: 20161022]

Matsuo R, Inoue T, Masuda Y, Nakamura O, Yamauchi Y, Morimoto T. Neural activity of chorda tympani mechanosensitive fibers during licking behavior in rats. Brain research. 1995; 689(2): 289–298. [PubMed: 7583333]

May OL, Erisir A, Hill DL. Ultrastructure of primary afferent terminals and synapses in the rat nucleus of the solitary tract: comparison among the greater superficial petrosal, chorda tympani, and glossopharyngeal nerves. The Journal of comparative neurology. 2007; 502(6):1066–1078. [PubMed: 17444498]

May OL, Hill DL. Gustatory terminal field organization and developmental plasticity in the nucleus of the solitary tract revealed through triple-fluorescence labeling. The Journal of comparative neurology. 2006; 497(4):658–669. [PubMed: 16739199]

McPheeters M, Hettinger TP, Nuding SC, Savoy LD, Whitehead MC, Frank ME. Taste-responsive neurons and their locations in the solitary nucleus of the hamster. Neuroscience. 1990; 34(3):745–758. [PubMed: 2352650]

Michael P, Raut V. Chorda tympani injury: operative findings and postoperative symptoms. Otolaryngol Head Neck Surg. 2007; 136(6):978–981. [PubMed: 17547991]

Miller AJ. Oral and pharyngeal reflexes in the mammalian nervous system: their diverse range in complexity and the pivotal role of the tongue. Crit Rev Oral Biol Med. 2002; 13(5):409–425. [PubMed: 12393760]

Nasse J, Terman D, Venugopal S, Hermann G, Rogers R, Travers JB. Local circuit input to the medullary reticular formation from the rostral nucleus of the solitary tract. Am J Physiol Regul Integr Comp Physiol. 2008; 295(5):R1391–R1408. [PubMed: 18716034]

Nejad MS. The neural activities of the greater superficial petrosal nerve of the rat in response to chemical stimulation of the palate. Chemical senses. 1986; 11:283–293.

Ninomiya Y. Salt taste responses of mouse chorda tympani neurons: evidence for existence of two different amiloride-sensitive receptor components for NaCl with different temperature dependencies. Journal of neurophysiology. 1996; 76(5):3550–3554. [PubMed: 8930292]

Norgren R. Projections from the nucleus of the solitary tract in the rat. Neuroscience. 1978; 3(2):207–218. [PubMed: 733004]

Norgren R. The gustatory system in mammals. Am J Otolaryngol. 1983; 4(4):234–237. [PubMed: 6312827]

Norgren, R. Central neural mechanisms of taste. In: Brookhart, JM., editor. Handbook of Physiology. 1984. p. 1087-1128.

Norgren R, Leonard CM. Ascending central gustatory pathways. The Journal of comparative neurology. 1973; 150(2):217–237. [PubMed: 4723066]

Ogawa H, Sato M, Yamashita S. Multiple sensitivity of chordat typani fibres of the rat and hamster to gustatory and thermal stimuli. J Physiol. 1968; 199(1):223–240. [PubMed: 5684036]

Paxinos, G.; Watson, C. The Rat Brain in Stereotaxic Coordinates. San Francisco, CA: Academic Press; 2009.

Perez R, Fuoco G, Dorion JM, Ho PH, Chen JM. Does the chorda tympani nerve confer general sensation from the tongue? Otolaryngol Head Neck Surg. 2006; 135(3):368–373. [PubMed: 16949966]

Renehan WE, Jin Z, Zhang X, Schweitzer L. Structure and function of gustatory neurons in the nucleus of the solitary tractI. A classification of neurons based on morphological features. The Journal of comparative neurology. 1994; 347(4):531–544. [PubMed: 7814673]

Renehan WE, Jin Z, Zhang X, Schweitzer L. Structure and function of gustatory neurons in the nucleus of the solitary tract: II. Relationships between neuronal morphology and physiology. The Journal of comparative neurology. 1996; 367(2):205–221. [PubMed: 8708005]

Schmued L, Slikker W Jr. Black-gold: a simple, high-resolution histochemical label for normal and pathological myelin in brain tissue sections. Brain research. 1999; 837(1–2):289–297. [PubMed: 10434014]

Schmued LC. A rapid, sensitive histochemical stain for myelin in frozen brain sections. J Histochem Cytochem. 1990; 38(5):717–720. [PubMed: 1692056]

Smith KG, Yates JM, Robinson PP. The effect of nerve growth factor on functional recovery after injury to the chorda tympani and lingual nerves. Brain research. 2004; 1020(1–2):62–72. [PubMed: 15312788]

Sollars SI, Hill DL. Lack of functional and morphological susceptibility of the greater superficial petrosal nerve to developmental dietary sodium restriction. Chemical senses. 2000; 25(6):719–727. [PubMed: 11114150]

Sollars SI, Hill DL. In vivo recordings from rat geniculate ganglia: taste response properties of individual greater superficial petrosal and chorda tympani neurones. J Physiol. 2005; 564(Pt 3): 877–893. [PubMed: 15746166]

Sollars SI, Walker BR, Thaw AK, Hill DL. Age-related decrease of the chorda tympani nerve terminal field in the nucleus of the solitary tract is prevented by dietary sodium restriction during development. Neuroscience. 2006; 137(4):1229–1236. [PubMed: 16338076]

Steele CM, Miller AJ. Sensory Input Pathways and Mechanisms in Swallowing: A Review. Dysphagia. 2010

Suwabe T, Bradley RM. Characteristics of rostral solitary tract nucleus neurons with identified afferent connections that project to the parabrachial nucleus in rats. Journal of neurophysiology. 2009; 102(1):546–555. [PubMed: 19439671]

Thomas JE, Hill DL. The effects of dietary protein restriction on chorda tympani nerve taste responses and terminal field organization. Neuroscience. 2008; 157(2):329–339. [PubMed: 18845228]

Torvik A. Afferent connections to the sensory trigeminal nuclei, the nucleus of the solitary tract and adjacent structures; an experimental study in the rat. The Journal of comparative neurology. 1956; 106(1):51–141. [PubMed: 13398491]

Travers JB. Efferent projections from the anterior nucleus of the solitary tract of the hamster. Brain research. 1988; 457(1):1–11. [PubMed: 3167557]

Travers SP, Hu H. Extranuclear projections of rNST neurons expressing gustatoryelicited Fos. The Journal of comparative neurology. 2000; 427(1):124–138. [PubMed: 11042595]

Travers SP, Norgren R. Organization of orosensory responses in the nucleus of the solitary tract of rat. Journal of neurophysiology. 1995; 73(6):2144–2162. [PubMed: 7666129]

van Giersbergen PL, Palkovits M, De Jong W. Involvement of neurotransmitters in the nucleus tractus solitarii in cardiovascular regulation. Physiol Rev. 1992; 72(3):789–824. [PubMed: 1352638]

Wang L, Bradley RM. In vitro study of afferent synaptic transmission in the rostral gustatory zone of the rat nucleus of the solitary tract. Brain research. 1995; 702(1–2):188–198. [PubMed: 8846076]

Whitehead MC. Anatomy of the gustatory system in the hamster: synaptology of facial afferent terminals in the solitary nucleus. The Journal of comparative neurology. 1986; 244(1):72–85. [PubMed: 3950091]

Whitehead MC. Neuronal architecture of the nucleus of the solitary tract in the hamster. The Journal of comparative neurology. 1988; 276(4):547–572. [PubMed: 2461969]

Whitehead MC. Subdivisions and neuron types of the nucleus of the solitary tract that project to the parabrachial nucleus in the hamster. The Journal of comparative neurology. 1990; 301(4):554–574. [PubMed: 2177063]

Whitehead, MC.; Finger, TE. Gustatory Pathways in Fish and Mammals. In: Firestein, S.; Beauchamp, GK., editors. The Senses: A Comprehensive Reference. Oxford, UK: Academic Press; 2008. p. 237-259.

Whitehead MC, Frank ME. Anatomy of the gustatory system in the hamster: central projections of the chorda tympani and the lingual nerve. The Journal of comparative neurology. 1983; 220(4):378–395. [PubMed: 6643734]

Whiteside B. Nerve overlap in the gustatory apparatus of the rat. The Journal of comparative neurology. 1927; 44:363–377.

Williams JB, Murphy DM, Reynolds KE, Welch SJ, King MS. Demonstration of a bilateral projection from the rostral nucleus of the solitary tract to the medial parabrachial nucleus in rat. Brain research. 1996; 737(1–2):231–237. [PubMed: 8930370]

Yamamoto T, Kawamura Y. Dual Innervation of the Foliate Papillae of the Rat: An Electrophysiological Study. Chemical Senses and Flavor. 1975; 1:241–244.

Yamashita S, Sato M. The effects of temperature on gustatory response of rats. J Cell Physiol. 1965; 66(1):1–17. [PubMed: 5857910]

Zaidi FN, Todd K, Enquist L, Whitehead MC. Types of taste circuits synaptically linked to a few geniculate ganglion neurons. The Journal of comparative neurology. 2008; 511(6):753–772. [PubMed: 18925565]

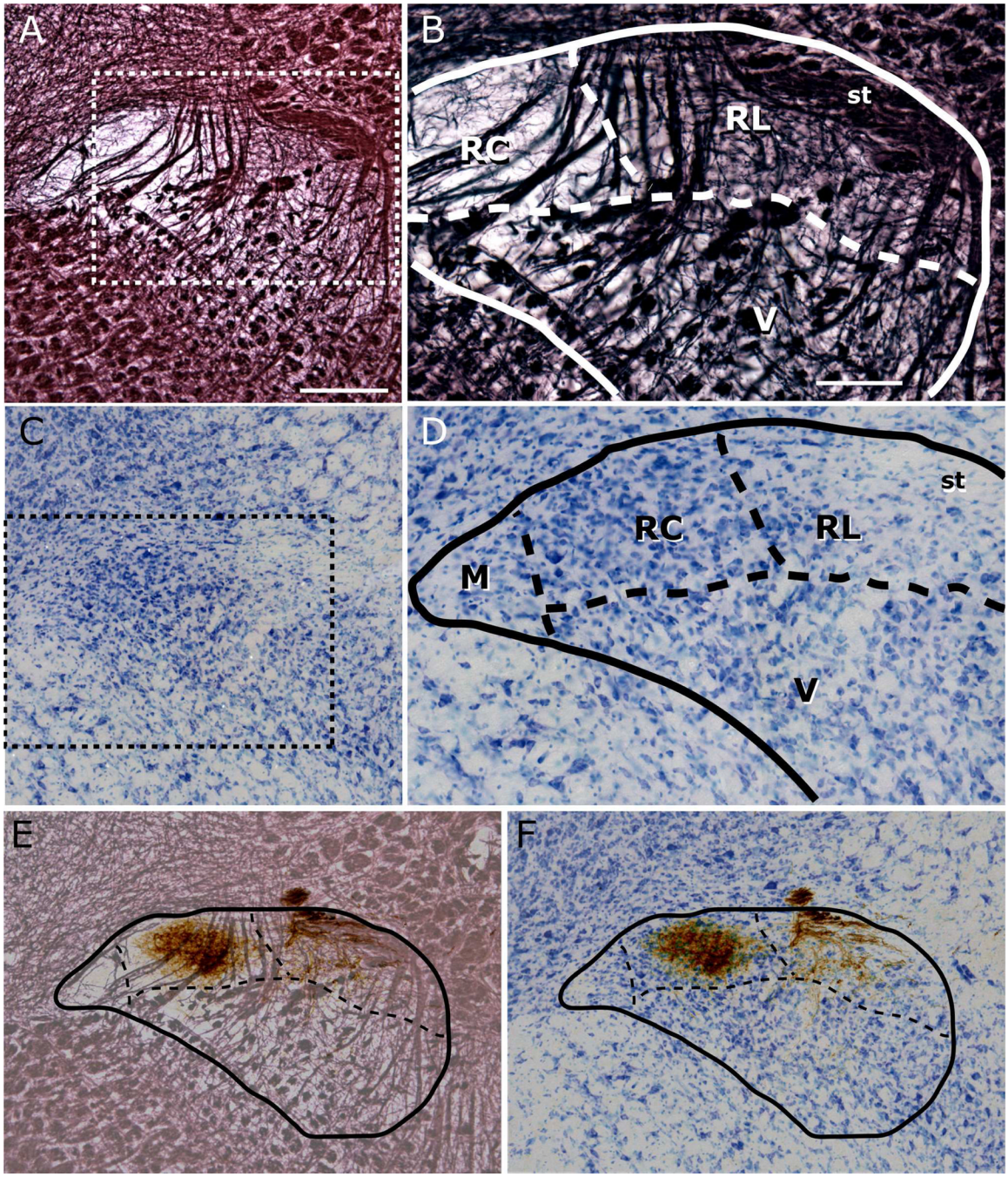

Figure 1.

Adjacent sections through rostral NTS, stained for myelin (panels A–B) and Nissl (panels C–D). The dashed box in panels A and C marks the region shown in panels B and D, respectively. Myelin staining delineates the dorsal and medial borders of the NTS, In myelin-stained sections, a distinct transition in patterns of fiber arrangement marks the border between rostrocentral (RC) and rostrolateral (RL) subdivisions (panel B). The border of the ventral (V) subdivision is demarcated as the dorsal extent of anterior-posterior traversing myelinated bundles. Differences in cell sizes and packing density visualized with Nissl provide landmarks for borders of several subdivisions (panels C–D), including between rostrocentral (RC) and rostrolateral (RL), and rostrocentral and medial (M). All

borders identified in each myelin-Nissl pair are transposed onto each other and then onto the tracer labeled adjacent section (panels E and F) to identify subdivision selective localization of afferent terminals. Illustrated here is a case with CT nerve labeling. Note that no sections were double-labeled. Scale in panel A = 250μm, and also applies to panels C, E, and F; scale in panel B =100μm, and also applies to panel D. st = solitary tract.

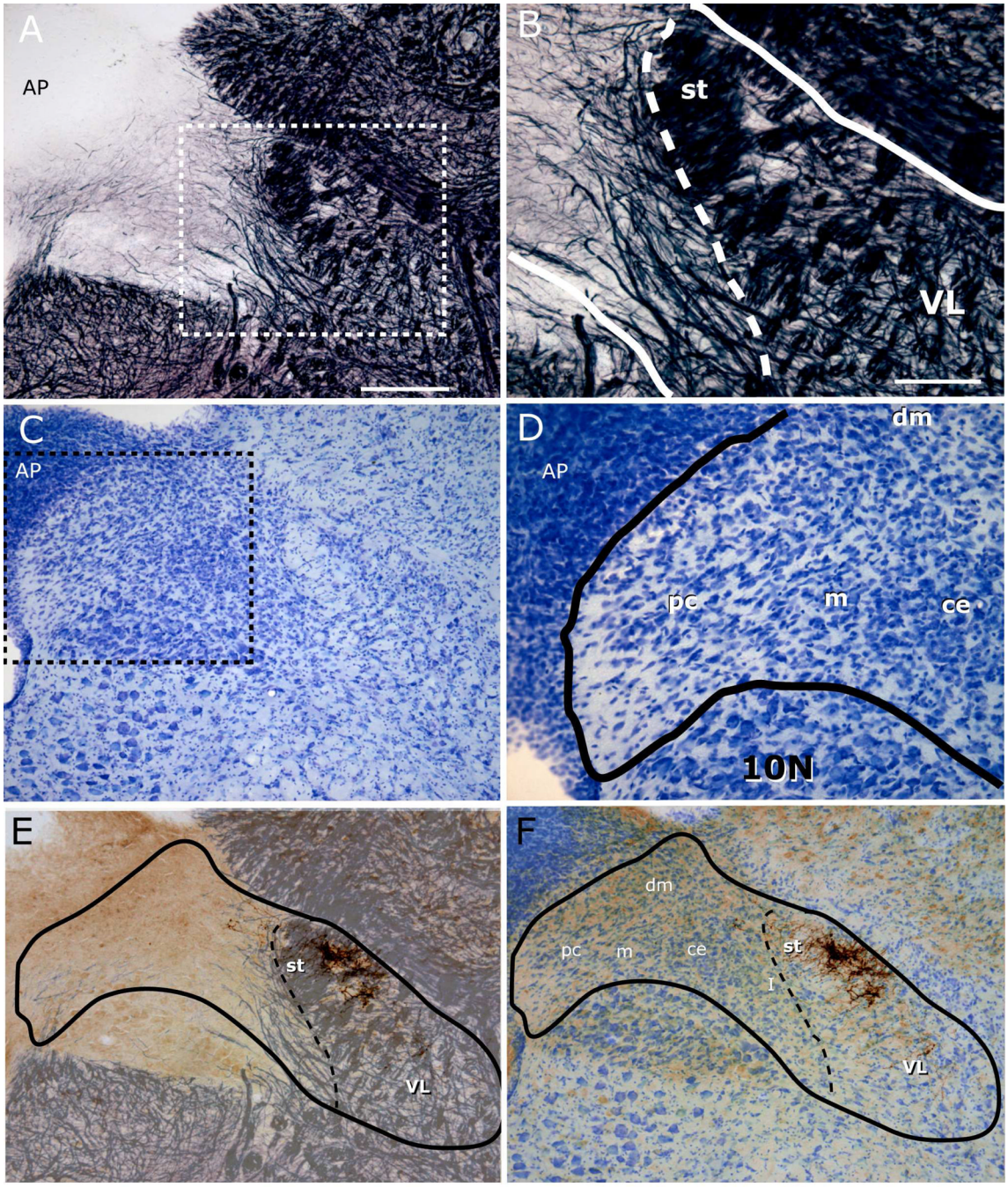

Figure 2.

Adjacent sections through caudal NTS, stained for myelin (panels A–B) and Nissl (panels C–D). The dashed box in panels A and C marks the region shown in panels B and D, respectively. The dorsal NTS border is delineated with myelin stain, medial border with area postrema (AP) or 4th ventricle (in the case of intermediate level sections), and the medial half of the ventral border with dorsal motor vagal nucleus (10N), which contains large cell bodies (panel D). Myelin staining delineates the border between the ventrolateral (VL) subdivision and the remainder of the NTS (panel B). Panels E–F: Superimposition of GSP labeling on adjacent myelin- and Nissl-stained sections, on which nucleus and subdivision borders are identified. The caudal subnuclei identified in previous studies (Herbert et al.

1990) are marked in Panels D and F. As only the ventrolateral subdivision is identifiable from the myelin staining, the other subnuclei have been omitted from Panel E. ce = central, pc = parvicellular, m = medial, dm = dorsomedial, I = intermediate, st = solitary tract. Scale in panel A = 250μm, and also applies to panels C, E, and F; scale in panel B = 100μm, and also applies to panel D.

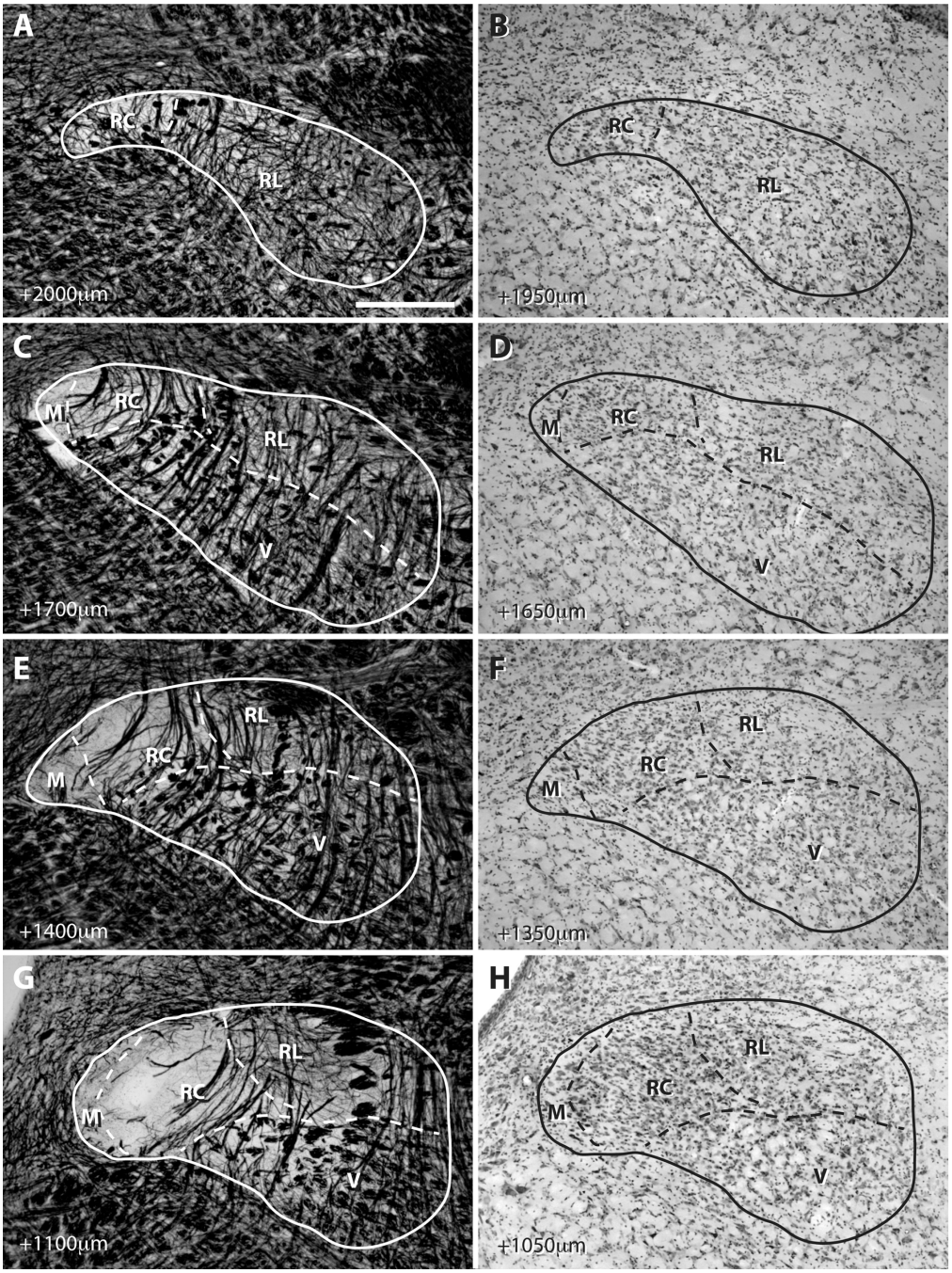

Figure 3.

The progression of NTS subdivisions through the rostral NTS from AP +2000μm to AP +1050μm as identified in adjacent myelin- and Nissl-stained sections. A–B): At the rostral-most portion of the NTS, the medial (M) and ventral (V) subdivisions are not identifiable. While, the delineation between rostrocentral (RC) and rostrolateral (RL) in the rostral-most section is somewhat ambiguous, the majority of NTS is histologically contiguous with RL in adjacent caudal sections. C–D): As the NTS progresses caudally, ventral and medial subdivisions, myelinated bundles of solitary tract and RC-RL border become identifiable. E–H: More posteriorly, the size of RC becomes larger, solitary tract attains the characteristic triangular shape, and ventral subdivision begin to secede to lateral. Although NTS shape and

absolute positions for subdivision borders vary among animals, the histological composition and pattern of progression of each subdivision are remarkably consistent. Scale in A = 280μm (applies to all panels).

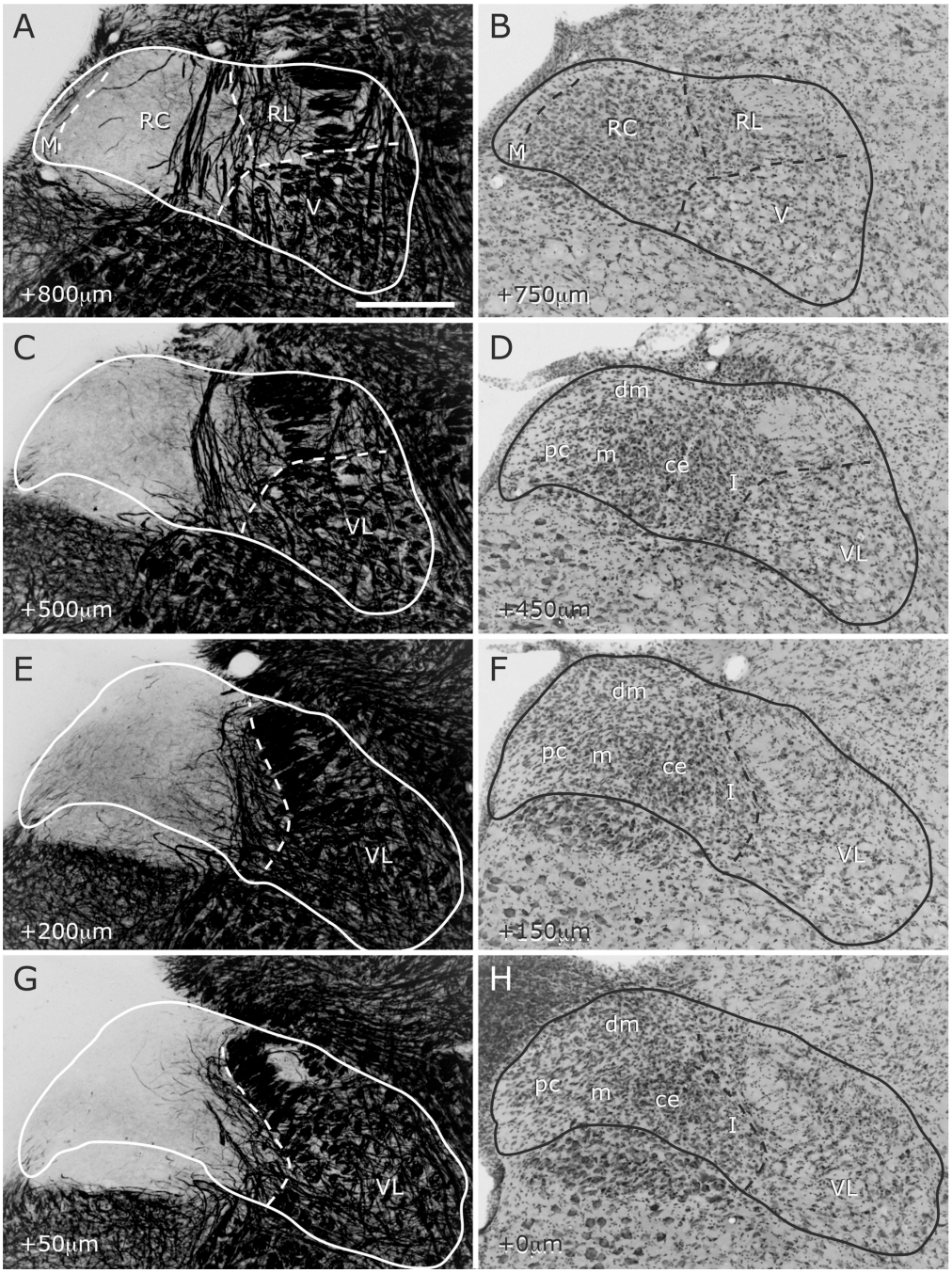

Figure 4.

The progression of NTS subdivisions through the caudal NTS from AP +800μm to AP +0μm as identified in adjacent myelin- and Nissl-stained sections. A–B: The level where the NTS joins the lateral wall of the 4th ventricle was operationally defined as the transition between the rostral and caudal NTS. As the histological constitution of the rostral-most section touching the 4th ventricle was similar to the remainder of the rostral NTS, the nomenclature in Figure 3 was maintained at this level (Whitehead, 1988). C–H: Caudal to the NTS-4th ventricle junction, the nomenclature of Herbert et al. 1990 was used. The border between the ventrolateral subdivision and the medial half of the NTS was identifiable in both myelin- and Nissl-stained sections and was demarcated by the dashed line. As with

rostral sections, NTS shape and absolute positions for subdivision borders vary among animals, yet the histological composition and pattern of progression of each subdivision are consistent. See Figure 2 for abbreviations. 10N = dorsal motor nucleus of the vagus. Scale in A = 280μm (applies to all panels).

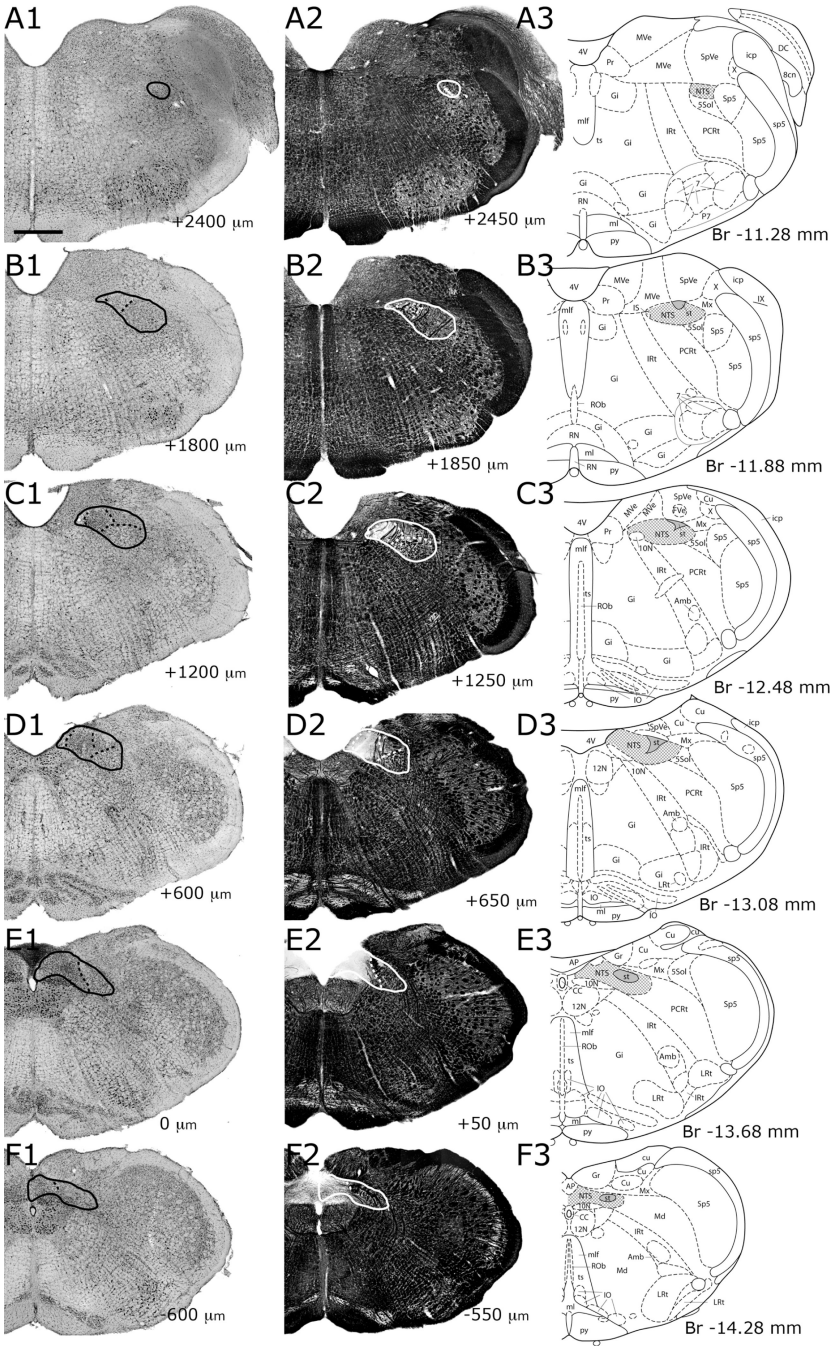

Figure 5.

Progression of NTS subdivisions identified in sections stained for Nissl (A1–F1) and myelin (A2–F2); consecutive sections in each column are 600μm apart. The anatomical landmarks are labeled in panels A3–F3, utilizing corresponding anterior-posterior plates from Paxinos atlas (Paxinos and Watson, 2009) for each Nissl-myelin pair. NTS and subdivisions are outlined in panels A1–F2, and shaded in A3–F3. Abbreviations are as given in List of Abbreviations. The anterior-posterior level of each section is marked on the lower right corner of each panel; this measurement is relative to the anterior-most section containing area postrema (E1), positive and negative numbers indicating anterior and posterior directions, respectively. Note that only one AP = 0 section is present in each brain, and in

this particular brain, it appears in panel E1. This was the anterior-most section containing area postrema. The NTS-4th ventricle junction appeared in this animal at AP +900μm. Scale bar = 700μm.

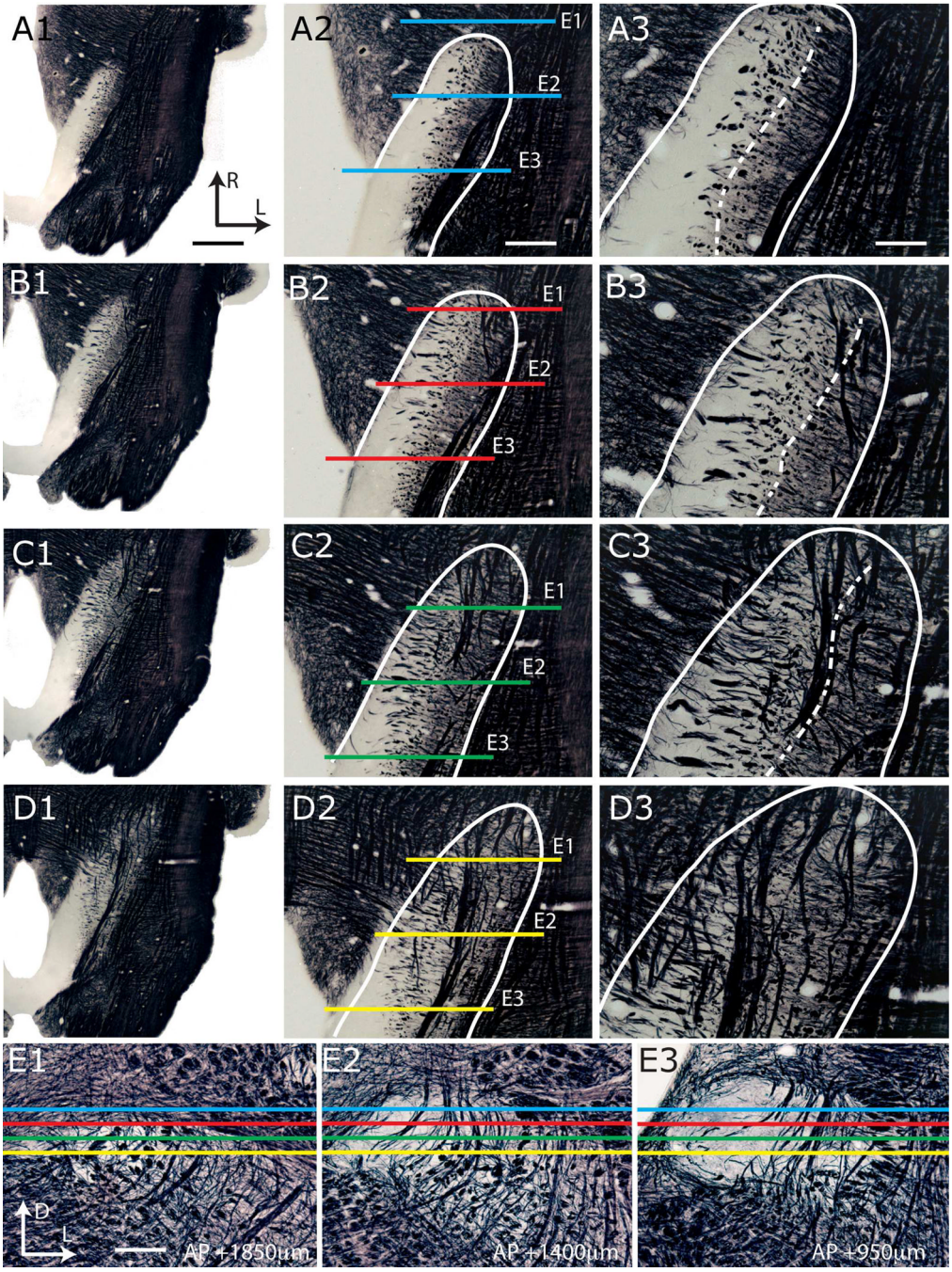

Figure 6.

Comparison of subdivision landmarks in horizontal and coronal planes in the NTS. Myelin staining of the NTS with four consecutive 50µm horizontal sections progressing ventrally (Rows A–D). Progressively higher resolutions are shown with the full brainstem in column 1 (A1–D1), the NTS from 4th-ventricle junction to rostral pole in column 2 (A2–D2; NTS outlined), and the rostral-most NTS in column 3 (A3–D3). Transition from myelinated axon bundles to fine myelin mesh delineates the rostrocentral-rostrolateral border (dashed white line; A3–C3). In row D, the RC-RL border delineation is absent as this section has progressed into the ventral subdivision. Row E shows myelin-stained coronal sections (450µm apart) between levels near the rostral pole and the NTS-4th ventricle junction. The

frames of panels A2–D2 color-code the dorsal-ventral level of each horizontal plane, and are indicated as dashed lines on coronal sections (E1–E3). Complementarily, anterior-posterior planes of coronal sections in E1, E2, and E3 are marked on horizontal sections in A2–D2 (orange lines), and labeled with corresponding coronal section panel number (E1, E2, or E3). These planes were determined by matching the known distance between sections and from the NTS-4th ventricle junction with the anterior-posterior extent of the NTS as viewed in the horizontal plane. Subdivision borders are omitted from coronal sections for ease of viewing (see Figures 1–5 for subdivision borders). Note that the most rostral portion of the NTS identified in coronal sections does not appear in dorsal horizontal sections (line labeled E1 in A1). Scales = 750μm in A1–D1; = 500μm in A2–D2; = 200μm in A3–D3 and E1–3. Axis abbreviations: R = Rostral, L = Lateral, D = Dorsal.

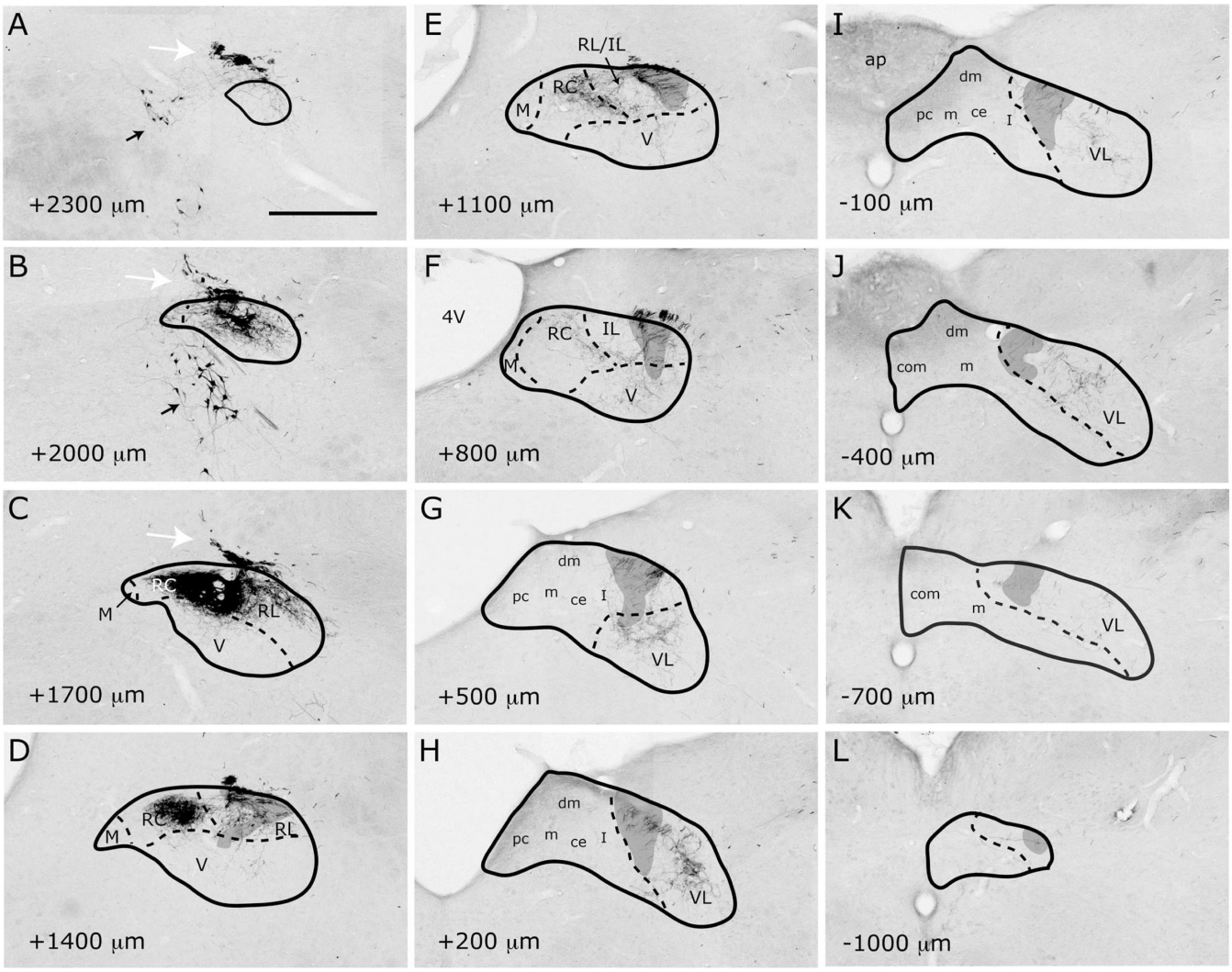

Figure 7.

Localization of labeled CT fibers in NTS subdivisions from the rostral pole (A) to the caudal-most section (L). NTS outlines and subdivision borders are transposed from adjacent Nissl- or myelin-stained sections for each panel. Bouton-bearing labeled fibers are found in sections from AP +2000μm (B) rostral to AP −400μm caudal (J). Prominent labeling is evident in the rostrocentral (B–E), rostrolateral (C–D) and ventrolateral (F–J) subdivisions. M = medial; RC = rostrocentral; RL = rostrolateral; V = ventral; VL = ventrolateral; IL = intermediate lateral; ce = central; pc = parvicellular; m = medial (from Herbert et al 1990); dm = dorsomedial; I = intermediate; com = commissural. ap = area postrema; 4V=4th ventricle. Shaded areas mark the solitary tract. White arrows = 7N. Black arrows = retrogradely filled efferent neurons. Scale bar = 500μm.

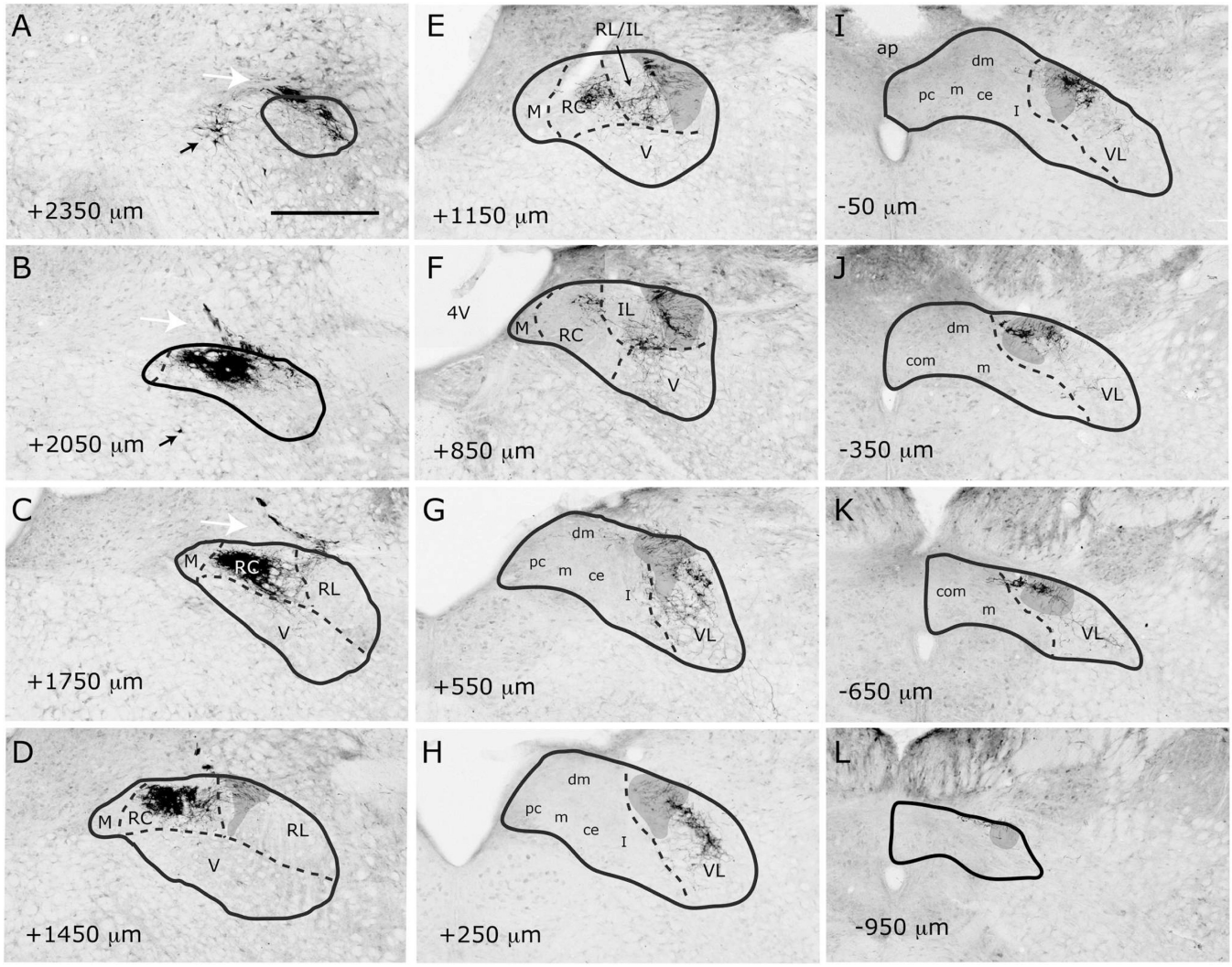

Figure 8.

Localization of labeled GSP fibers in NTS subdivisions from the rostral pole (A) to the caudal sections (L). NTS outlines and subdivision borders are transposed from adjacent Nissl- or myelin-stained sections for each panel. Bouton-bearing labeled fibers are found in sections from AP +2350μm (A) rostral to AP −650μm caudal (J). Prominent labeling is evident in the rostrocentral (B–E) and ventrolateral (F–J) subdivisions. Subdivision abbreviations are as in Figure 7. Shaded areas mark the solitary tract. White arrows = 7N. Black arrows = retrogradely filled efferent neurons. Scale bar = 500μm.

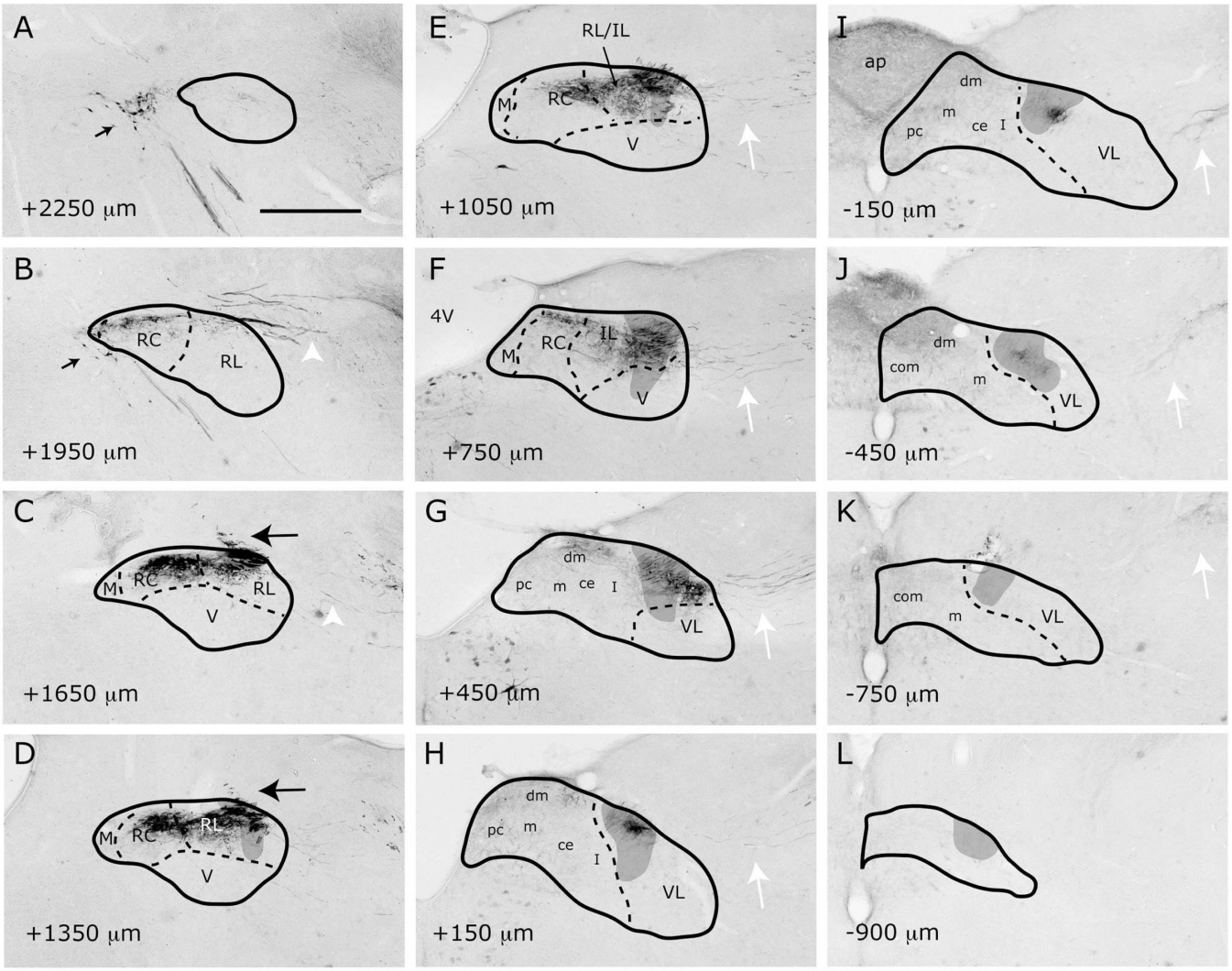

Figure 9.

Localization of labeled IX fibers in NTS subdivisions from the rostral pole (A) to the caudal sections (L). NTS outlines and subdivision borders are transposed from adjacent Nissl- or myelin-stained sections for each panel. Bouton-bearing labeled fibers are found in sections from AP +1650μm (C) rostral to AP +450μm caudal (G). Prominent labeling is evident in the rostrocentral (C–E), rostrolateral (C–E), intermediate lateral (E–F) and interstitial nucleus (F–H). The great majority of labeled fibers observed in caudal sections (G–J) are non-bouton bearing labeled axon bundles traveling within the solitary tract. Subdivision abbreviations are as in Figure 7. Shaded areas mark the solitary tract. White arrows mark several distinct bundles of IX fibers that enter NTS along its lateral aspect (E–K). White arrowheads mark a labeled axon bundle that approaches the NTS rostral pole (B–C) and enters NTS from its dorsal aspect (large black arrow). Small black arrows mark retrogradely filled efferent neurons in the inferior salivatory nucleus (A–B). Scale bar = 500μm.

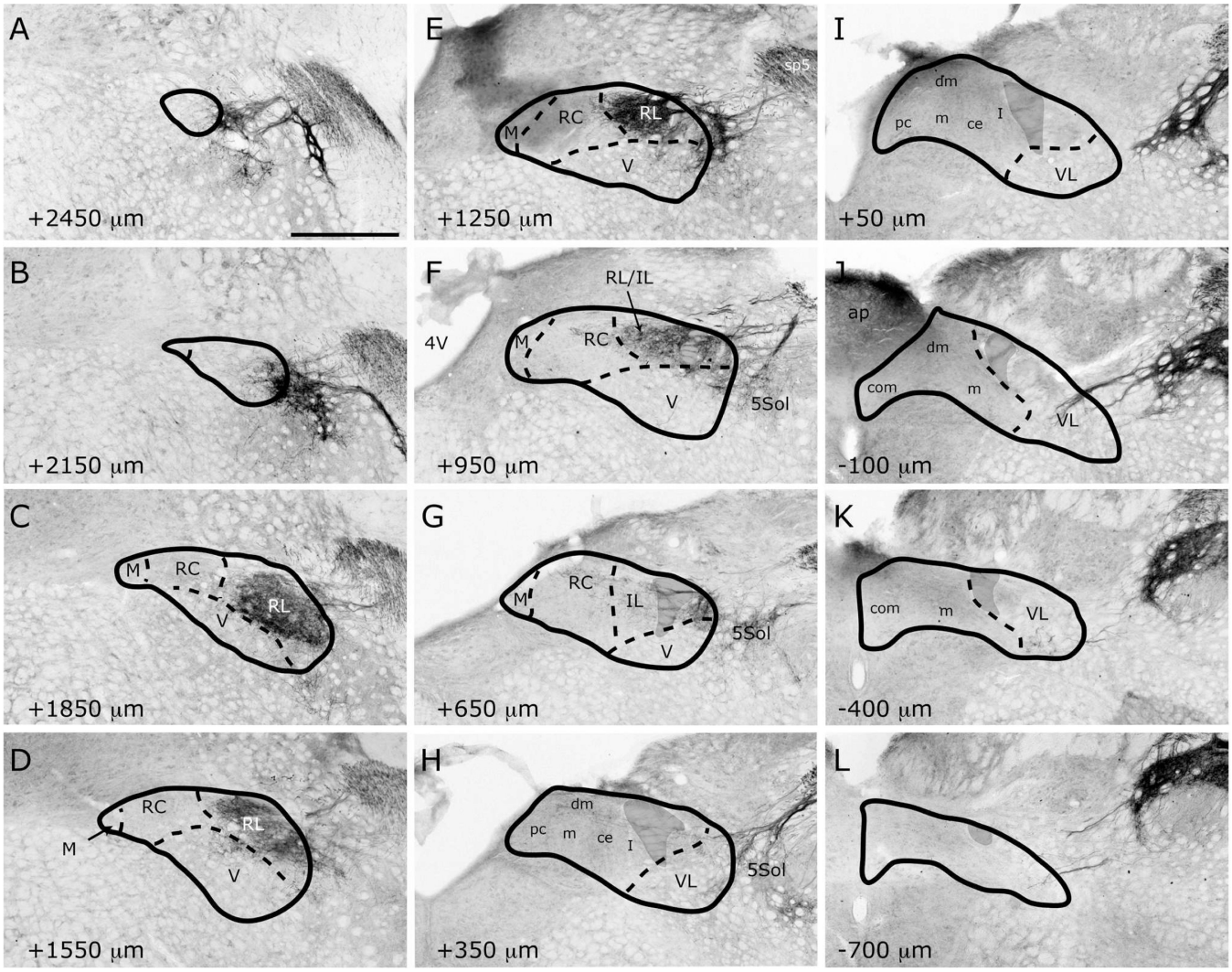

Figure 10.

Localization of labeled LV fibers in NTS subdivisions from the rostral pole (A) to the caudal sections (L). NTS outlines and subdivision borders are transposed from adjacent Nissl- or myelin-stained sections for each panel. Bouton-bearing labeled fibers are found throughout the rostral-caudal extent of the NTS, with the densest labeling appearing in sections from AP +2150μm (B) rostral to AP +950μm caudal (F). Prominent labeling is evident in the rostrolateral subdivision (C–F). Very sparse terminal field is present in the ventrolateral subdivision (H–L) throughout the caudal extent of the NTS. Subdivision abbreviations are as in Figure 7. Shaded areas mark the solitary tract. 5Sol = trigeminal-NTS transition zone. sp5= trigeminal tract. Scale bar = 500μm.

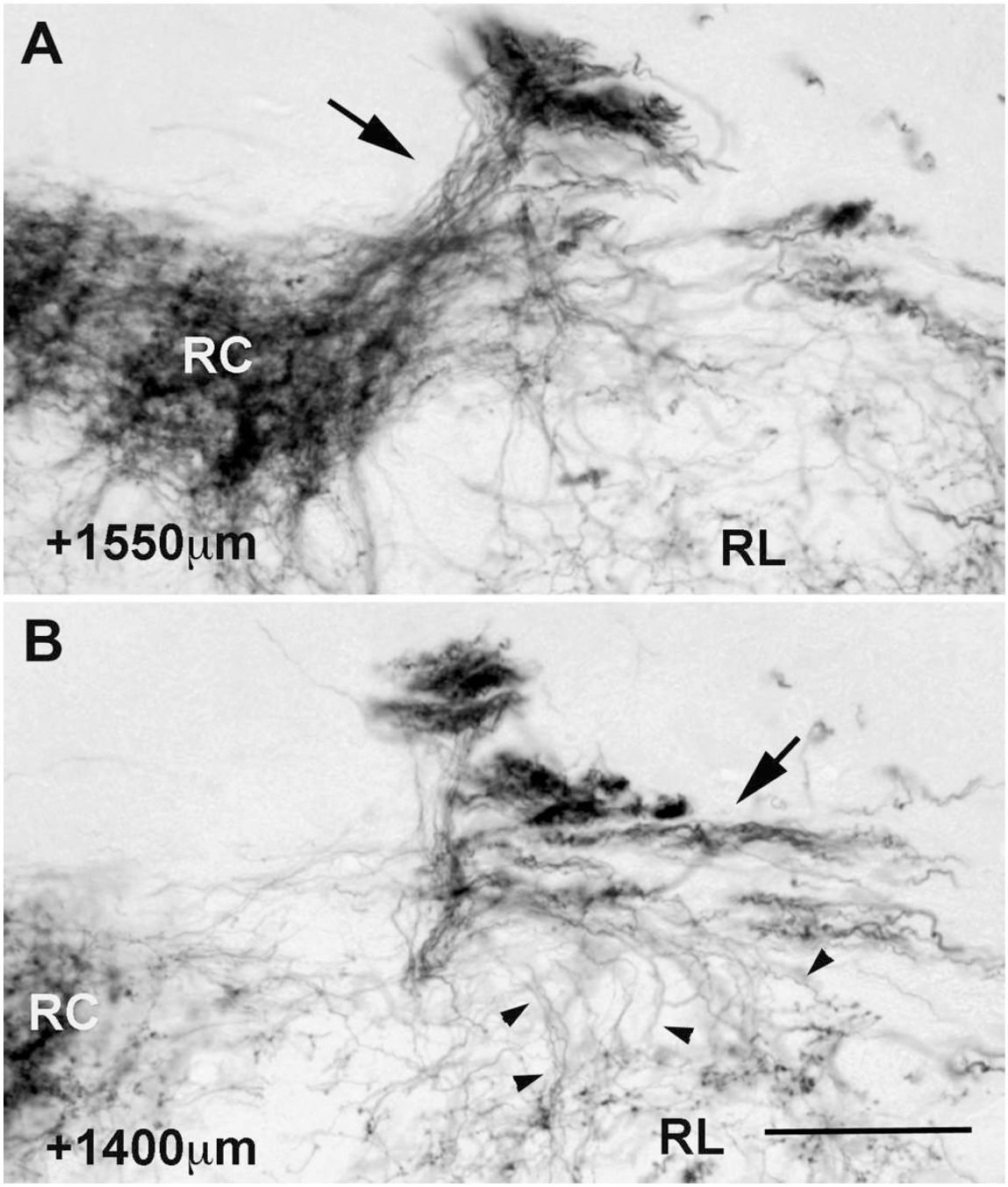

Figure 11.
CT innervation of the rostrocentral and rostrolateral subdivisions arises from different fiber bundles. At the coronal level containing the densest CT label (A) a large fiber bundle (arrow) travels in a ventral and medial orientation directly into the lateral most portion of the rostrocentral subdivision. This bundle then produces the terminal field in the rostrocentral subdivision. Approximately 150μm caudal (B) a second bundle (arrow) is traversing the dorsal border of the rostrolateral subdivision. Individual fibers (arrowheads) can be seen projecting ventrally off of this bundle into the rostrolateral subdivision. Scale = 150μm (same for A and B).

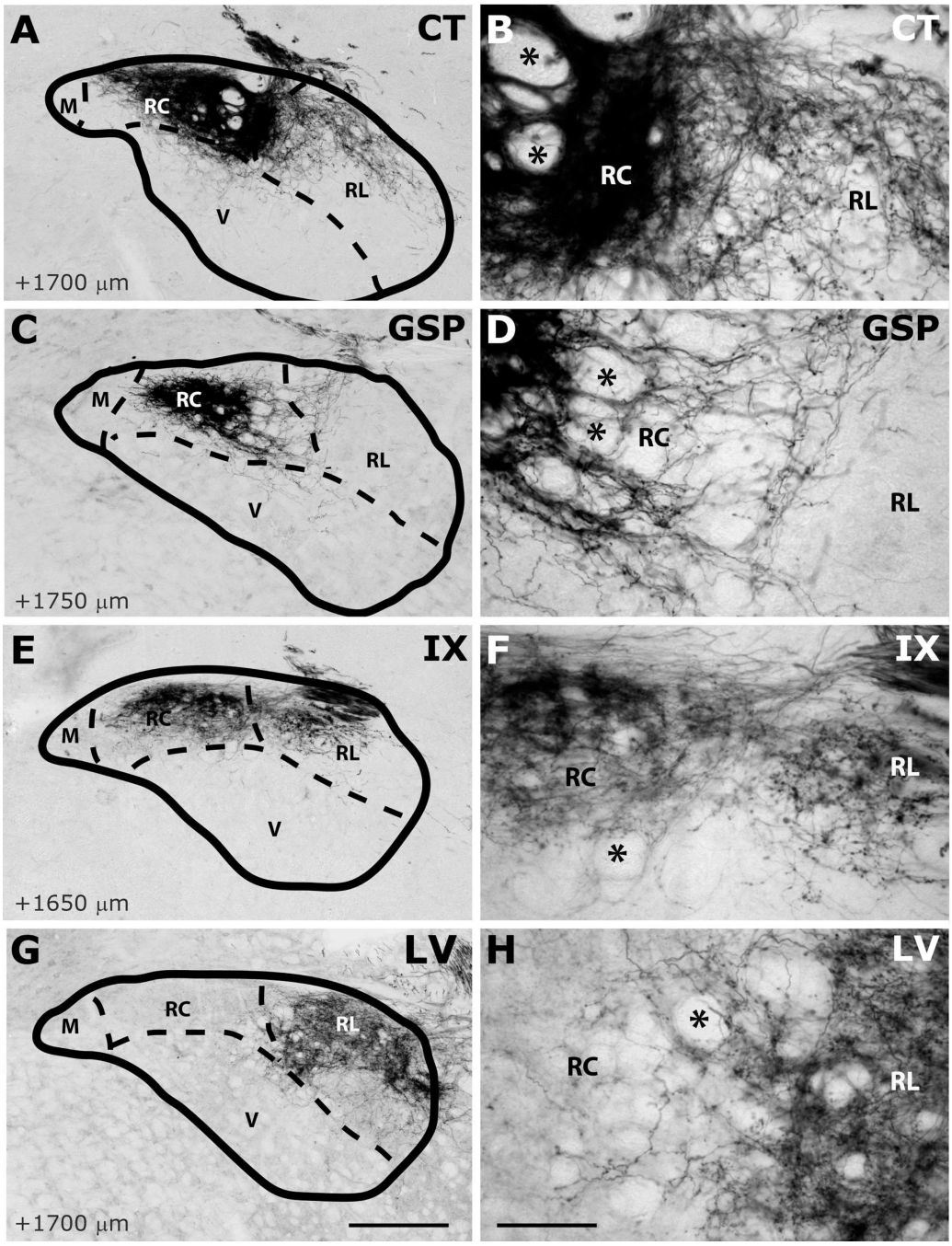

Figure 12.

Innervation of rostrocentral (RC) and rostrolateral (RL) subdivisions by CT (A–B), GSP (C–D), IX (E–F), and LV (G–H) fibers at approximately AP+1700μm. Panels B, D, F and H are higher magnification view of A, C, E and G, displaying labeling in RC and RL subdivisions. NTS and subdivision borders are superimposed from adjacent Nissl- and myelin-stained sections. Compared to CT, GSP fibers are more condensed in medial portions of the rostrocentral subdivision, and they are absent in rostrolateral subdivision. CT fibers occupy the dorsal and medial portions of the rostrolateral subdivision. IX fibers are sparser than the other two, and concentrated in the dorsal rostrocentral subdivision and a wider portion of the rostrolateral subdivision. LV fibers are confined within the rostrolateral subdivision.

Asterisks mark the void of anterior-posterior running axon bundles, which are found in comparable locations in all animals depicted. Scale in G = 250μm (also applies to A, C, E, and G). Scale in H = 60μm (also applies to B, D, F, and H).

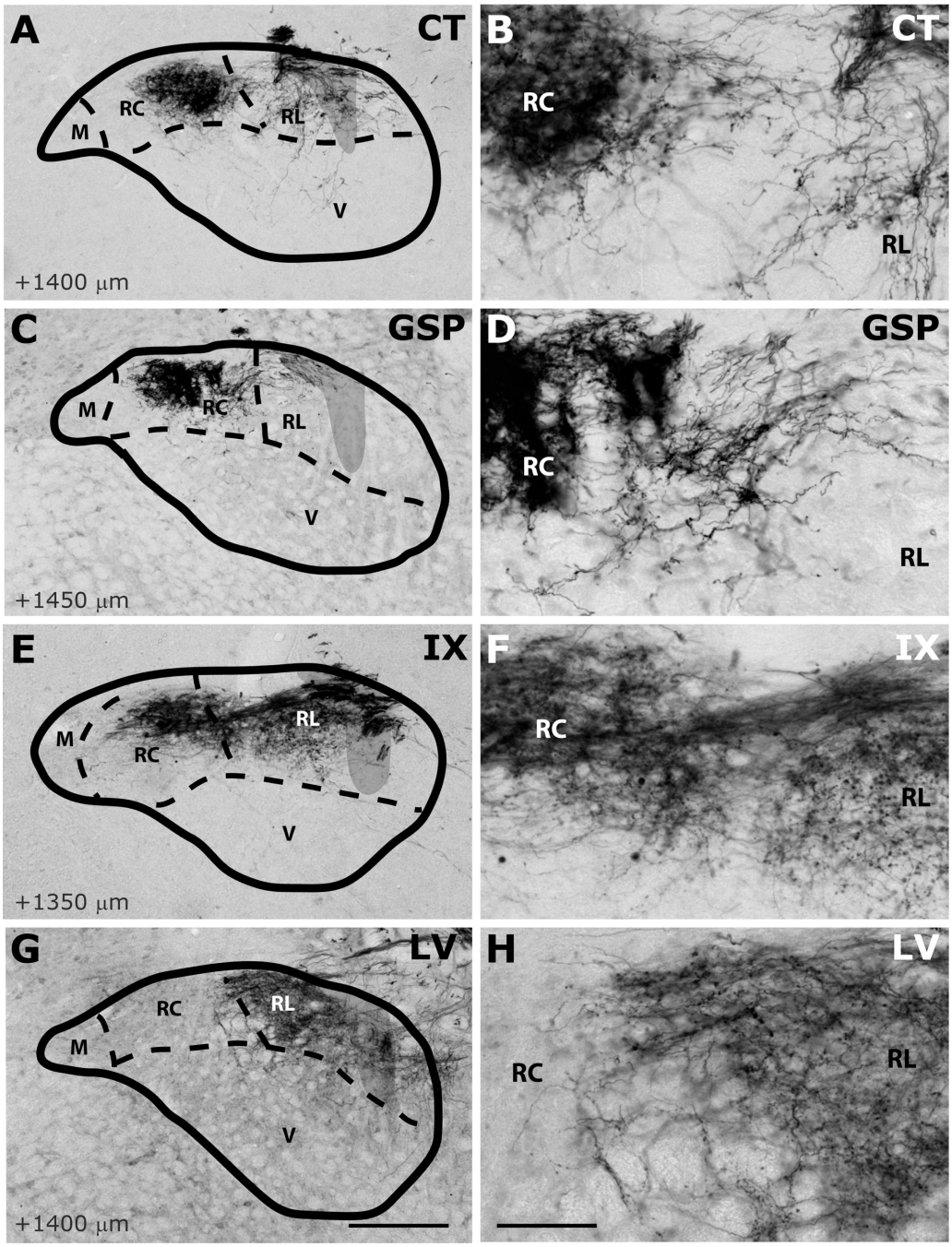

Figure 13.

Innervation of rostrocentral (RC) and rostrolateral (RL) subdivisions by CT (A–B), GSP (C–D), IX (E–F), and LV (G–H) fibers at AP+1400μm. Panels B, D, F and H are higher magnification view of A, C, E and G, displaying labeling in RC and RL subdivisions. NTS and subdivision borders are superimposed from adjacent Nissl- and myelin-stained sections. A distinct fiber free zone separates CT projections in RC and RL. GSP fibers are sparse at the lateral edge of RC, and absent from RL. IX fibers innervate both rostrocentral and rostrolateral densely. A bundle of IX fibers emerges from the large fascicule of labeled IX nerve that courses the dorsal surface of NTS, and extend into RC to form the terminal field (also see Figure 18). LV fibers are confined within the rostrolateral subdivision. Shaded

areas mark the solitary tract. Scale in G = 250μm (also applies to A, C, E, and G). Scale in H = 60μm (also applies to B, D, F, and H).

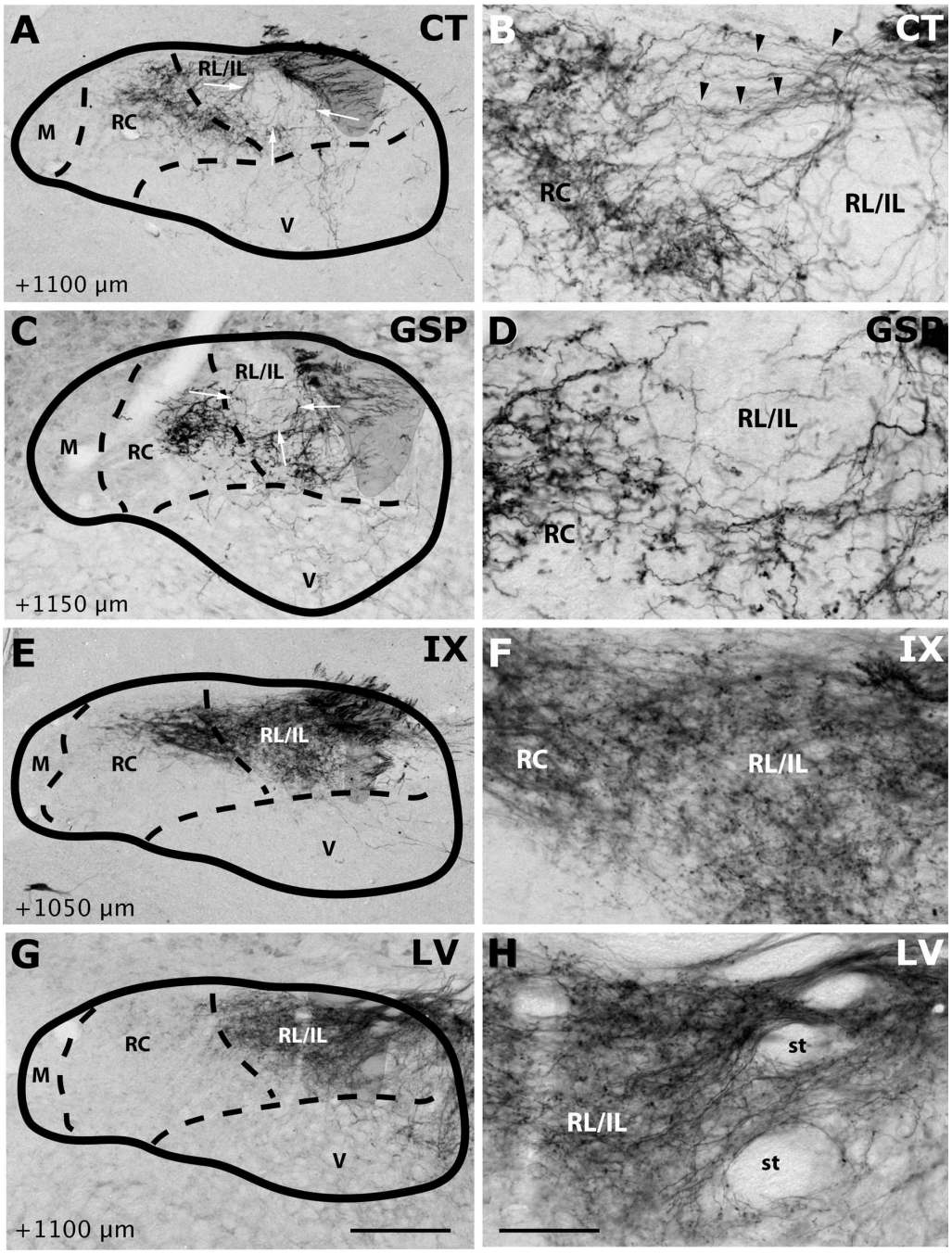

Figure 14.

Innervation of rostrocentral and rostrolateral/intermediate lateral subdivisions by CT (A–B), GSP (C–D), IX (E–F), and LV (G–H) fibers at approximately AP+1100μm. Panels B, D, F and H are higher magnification view of A, C, E and G, displaying labeling in the intermediate lateral subdivision. NTS and subdivision borders are superimposed from adjacent Nissl- and myelin-stained sections. CT and GSP fibers surround the medial and ventral borders of the intermediate lateral subdivision. As there are some scant CT and GSP fibers in this region at this coronal level and there are no histological boundaries between the rostrolateral and intermediate lateral subdivisions, this region has been marked RL/IL. Both IX and LV innervate the intermediate lateral subdivision. Shaded areas mark the solitary

tract. Scale in G = 250μm (also applies to A, C, E, and G). Scale in H = 60μm (also applies to B, D, F, and H). st = solitary tract.

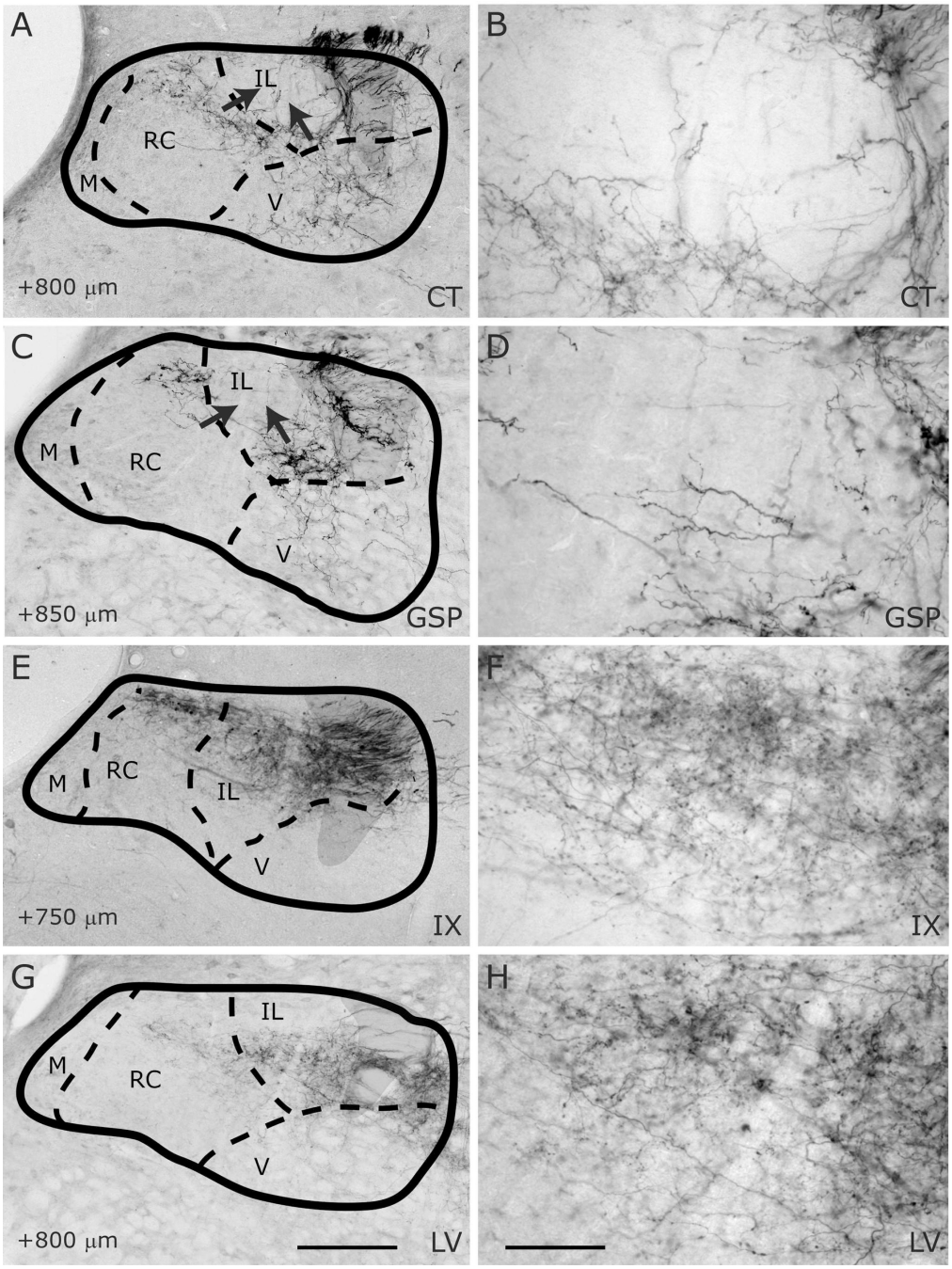

Figure 15.

Innervation of rostrocentral/caudocentral and intermediate lateral subdivisions by CT (A–B), GSP (C–D), IX (E–F), and LV (G–H) fibers at the rostral-caudal level of approximately AP +800μm. NTS and subdivision borders are superimposed from adjacent Nissl- and myelin-stained sections. Sparse CT and GSP fibers innervate the rostral-most portion of the rostrocentral subdivision, whereas IX fibers are denser. The CT and GSP fields surround a globular-shaped, intermediate lateral subdivision from its medial and ventral aspects (arrows in A and C). IX and LV fibers densely fill this intermediate lateral subdivision. CT and GSP fibers are also present in the ventral subdivision. Shaded areas mark the solitary tract. Scale

in G = 250μm (also applies to A, C, E, and G). Scale in H = 60μm (also applies to B, D, F, and H).

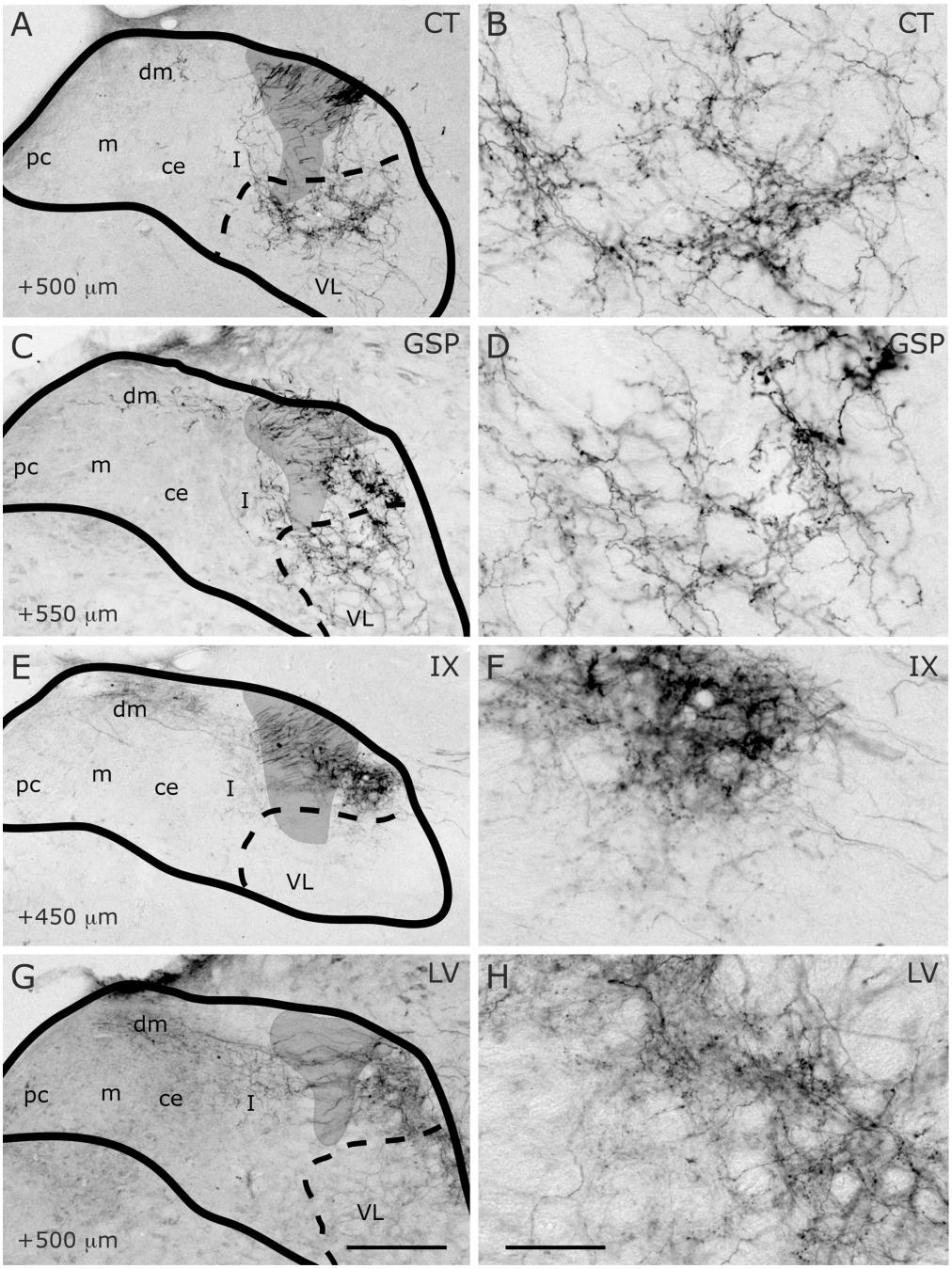

Figure 16.

Innervation of the ventrolateral subdivision by CT (A–B), GSP (C–D), IX (E–F), and LV (G–H) fibers at the rostral-caudal level at approximately AP+500μm. NTS and subdivision borders are superimposed from adjacent Nissl- and myelin-stained sections. IX innervates the rostral-most portion of dorsomedial subnucleus, though this may actually be the caudal-most extent of the rostrocentral subdivision (Panel E & F, black arrow heads mark the incoming IX fibers, white arrows mark terminal bouton bearing axons). The same region also receives GSP and LV but not CT innervation, consistent with further compartmentalization within CL. LV extends ventrally along the lateral border of the ventrolateral subdivision. Distinctly bouton-bearing fibers from CT and GSP nerves are also

found in the ventrolateral subdivision. Shaded areas mark the solitary tract. Scale in G = 250μm (also applies to A, C, E, and G). Scale in H = 60μm (also applies to B, D, F, and H).

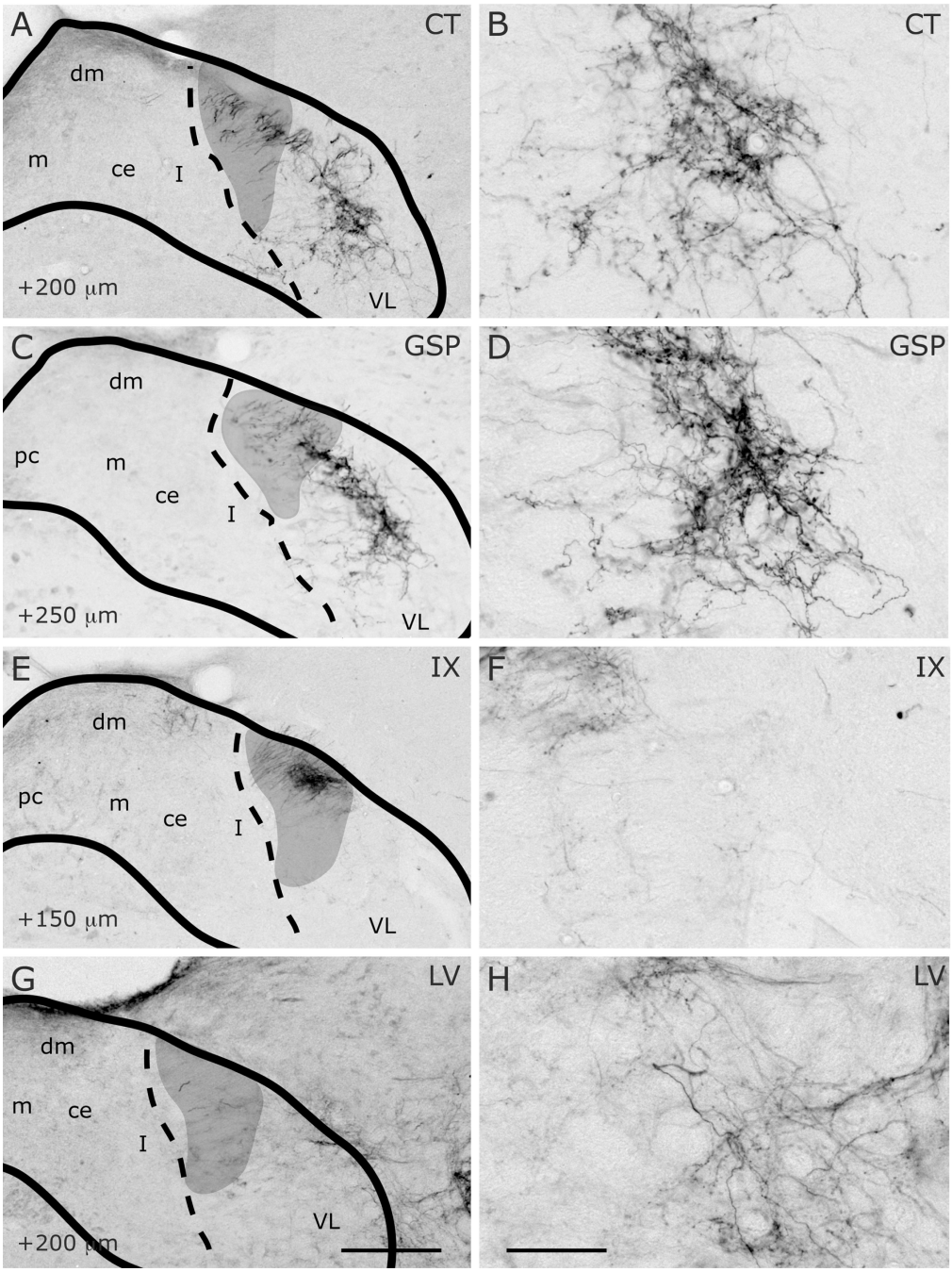

Figure 17.

Innervation of the ventrolateral subdivision by CT (A–B), GSP (C–D), IX (E–F), and LV (G–H) fibers at the rostral-caudal level of approximately AP+200μm. NTS and subdivision borders are superimposed from adjacent Nissl- and myelin-stained sections. CT and GSP innervate a distinct region in the middle of the ventrolateral subdivision. IX and LV largely avoid this region. LV fibers and terminal field located along the lateral border of the ventrolateral subdivision. Shaded areas mark the solitary tract. Scale in G = 250μm (also applies to A, C, E, and G). Scale in H = 60μm (also applies to B, D, F, and H).

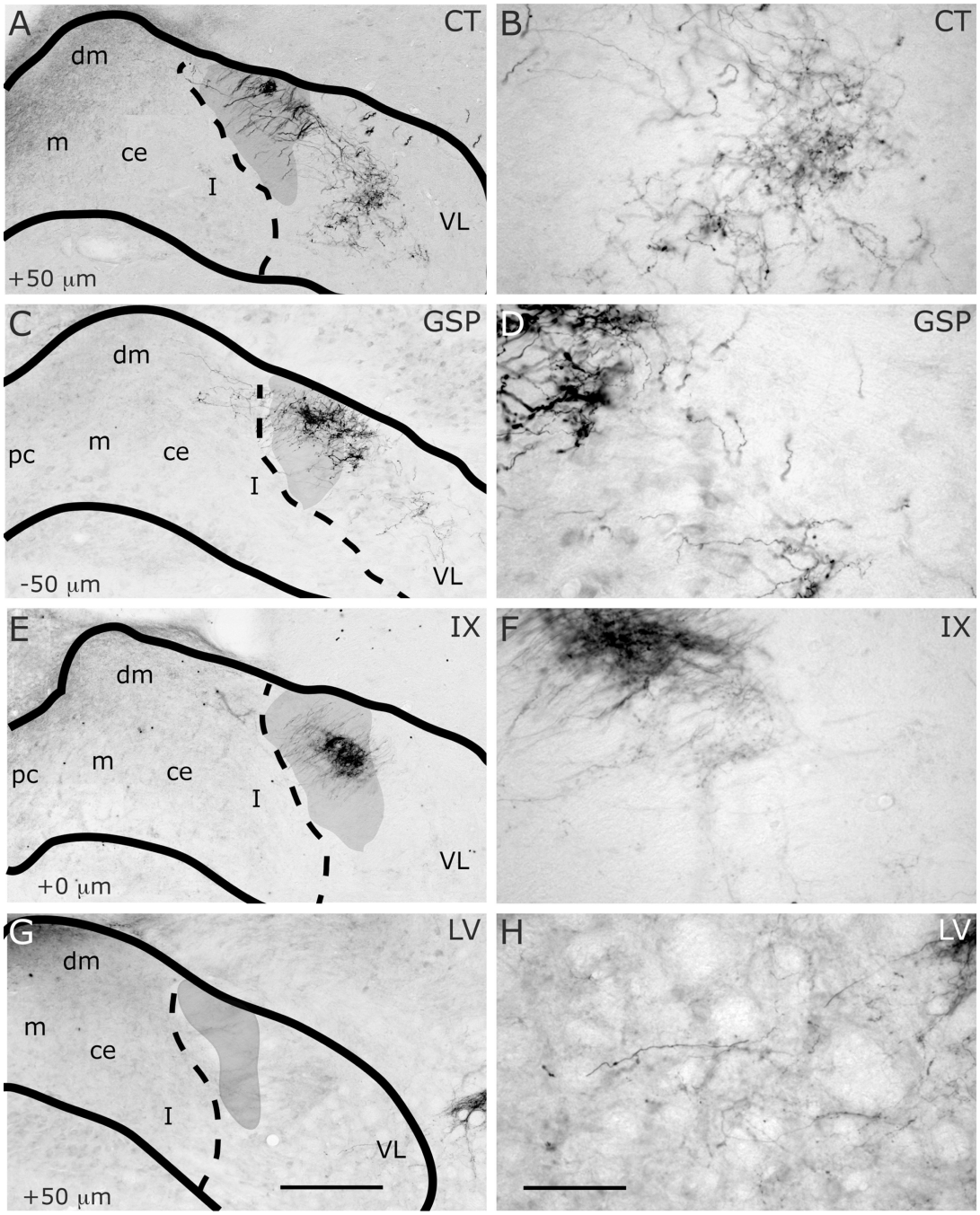

Figure 18.

Innervation of ventrolateral subdivision by CT (A–B), GSP (C–D), IX (E–F), and LV (G–H) fibers at the rostral-caudal level at approximately AP+0μm. NTS and subdivision borders are superimposed from adjacent Nissl- and myelin-stained sections. Unlike CT and GSP fields, which innervate the ventrolateral subdivision, non-bouton bearing IX fibers are only, and sparsely, present within the solitary tract. Sparse bouton bearing fibers from IX and GSP can be seen along the lateral wall of the solitary tract in the interstitial nucleus (in). CT and GSP innervate a specific region of the ventrolateral subdivision, the boundaries of which are not discernable from this histologically stained material. LV fibers innervate the ventrolateral subdivision sparsely and irregularly. At this anterior-posterior level, no terminal field

labeling is present in any other subdivision. Shaded areas mark the solitary tract. Scale in G = 250μm (also applies to A, C, E, and G). Scale in H = 60μm (also applies to B, D, F, and H).

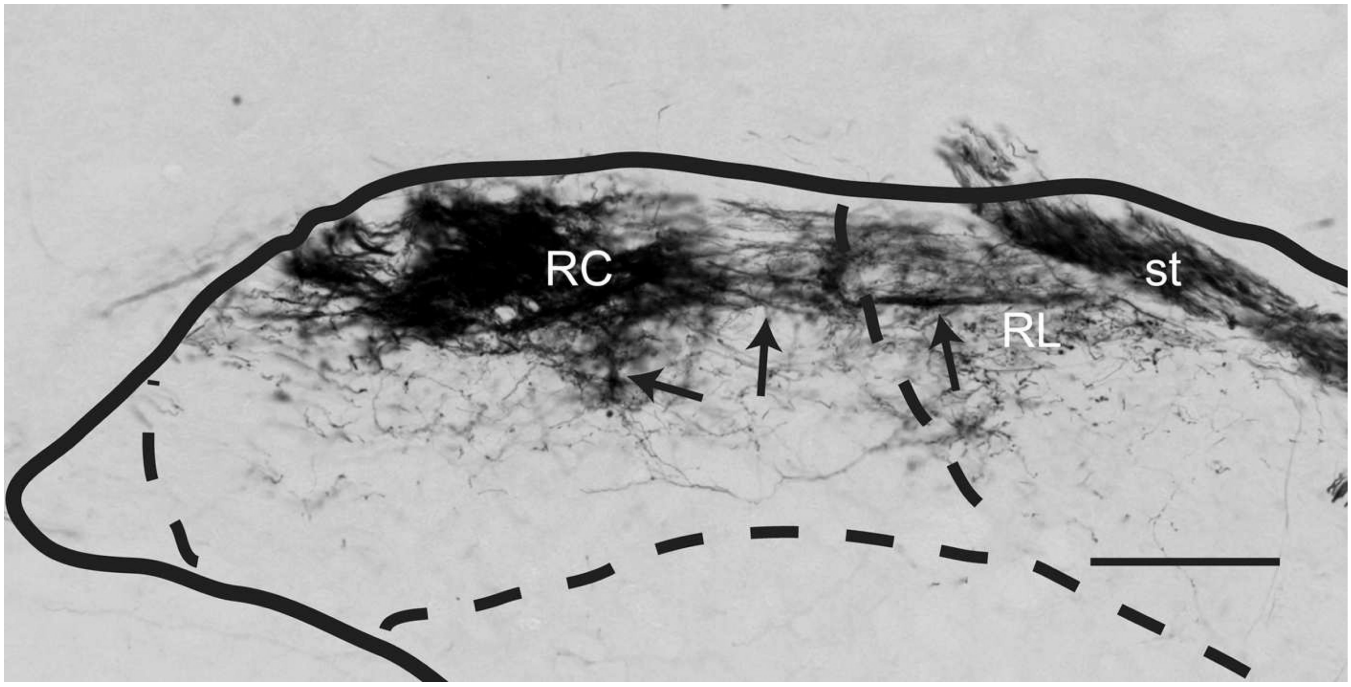

Figure 19.
IX fibers innervate the NTS through the lateral border, enter the solitary tract, and course laterally through the NTS. From here, non-bouton bearing bundles of fibers (arrows) can be seen travelling along the dorsal aspect of the nucleus, sending projections ventrally into the rostrolateral (RL) and rostrocentral (RC) subdivisions. Both subdivisions appear to be filled with large caliber fibers as well as varicosities emanating from finer caliber axons. Scale = 150μm.

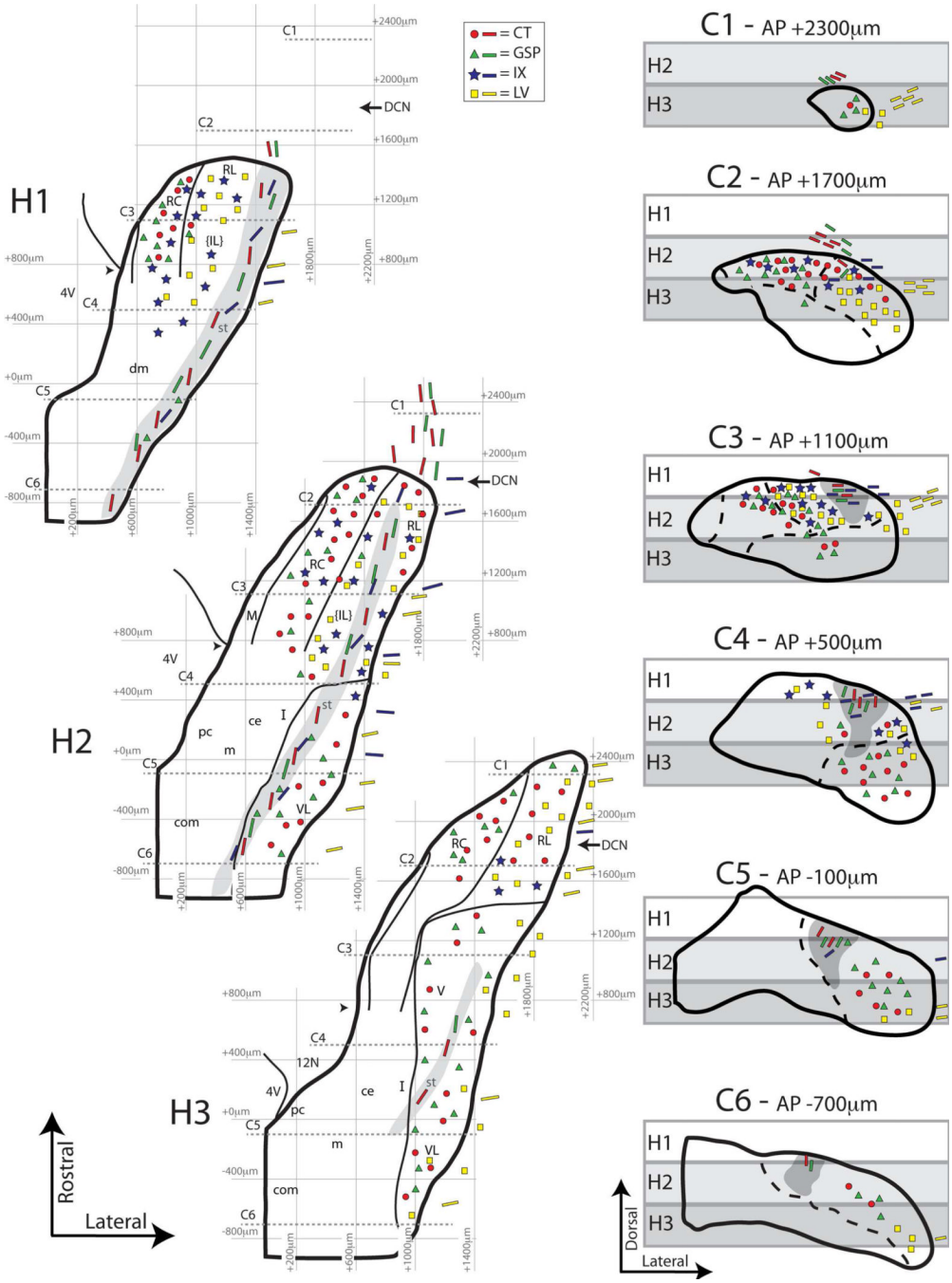

Figure 20.

Summary of subdivision borders and afferent labeling patterns in the NTS as viewed in both coronal and horizontal planes. A coronal series is mapped upon AP and brainstem surface anchored coordinates to obtain a numerical 3D construction of the NTS. Then, lateral and medial NTS borders in 200µm dorsal-ventral slabs were used to construct horizontal NTS sections comparable to those from studies utilizing the horizontal plane. Gray rectangles over representative coronal sections C1–C6 depict the placement of these three horizontal slabs (H1–H3). The dorsal (H1) intermediate (H2) and ventral (H3) thirds of the NTS are illustrated in horizontal planes constructed in this manner. H1, H2, and H3 planes correspond to 400–600µm, 600–800µm and 800–1000µm respectively from the brainstem

surface. Dotted grey lines in H1–H3 indicate corresponding coronal levels C1–C6. Subdivision borders (thin solid lines) and solitary tract (gray fill) are also converted from actual coronal sections to these simulated horizontal planes. Terminal field distributions in NTS subdivisions (as interpreted from the coronal atlases in Figures 6–9) are illustrated as markers (legend at top) in coronal sections C1–C6, and this information is further transferred onto simulated horizontal planes H1–H3. Note that the markers indicate that labeled fibers are present within given subdivisions, not the density of labeling or specific terminal bouton locations in any region. Non-bouton bearing fibers are marked as bars with corresponding nerve colors. The border between the rostral and caudal NTS is not indicated, as there are no clear histological boundaries between the two. As with previous figures, caudal NTS subnuclei based solely on Nissl staining are noted, but borders are not drawn. Red circles = chorda tympani (CT), green triangles = greater superficial petrosal (GSP), blue stars = glossopharyngeal (IX), yellow squares = lingual-trigeminal (LV). DCN = Anterior posterior level of the dorsal cochlear nucleus. 4V = Fourth ventricle (arrow head = level at which the NTS and fourth ventricle separate). RC = rostrocentral; RL = rostrolateral; M = medial; ce = central; pc = parvicellular; m = medial (from Herbert et al 1990); dm = dorsomedial; I = intermediate; com =commissural; IL = intermediate lateral (the brackets indicate that this is based on terminal field distribution rather than histologically identified borders). VL = ventrolateral. V = ventral.